Cell

Mixed Lineage Kinase Domain-like Protein Mediates Necrosis Signaling Downstream of RIP3 Kinase

Liming Sun,[1,2] Huayi Wang,[1,2] Zhigao Wang,[2] Sudan He,[1] She Chen,[1] Daohong Liao,[1,3] Lai Wang,[2] Jiacong Yan,[1] Weilong Liu,[1,4] Xiaoguang Lei,[1,3,*] and Xiaodong Wang[1,2,*]

[1]National Institute of Biological Sciences, 7 Science Park Road, Zhongguancun Life Science Park, Beijing 102206, China
[2]Department of Biochemistry, University of Texas Southwestern Medical Center, 5323 Harry Hines Boulevard, Dallas, TX 75390, USA
[3]School of Pharmaceutical Science and Technology, Tianjin University, Tianjin 300072, China
[4]Peking Union Medical College and Chinese Academy of Medical Sciences, Beijing 100730, China
*Correspondence: leixiaoguang@nibs.ac.cn (X.L.), wangxiaodong@nibs.ac.cn (X.W.)
DOI 10.1016/j.cell.2011.11.031

SUMMARY

The receptor-interacting serine-threonine kinase 3 (RIP3) is a key signaling molecule in the programmed necrosis (necroptosis) pathway. This pathway plays important roles in a variety of physiological and pathological conditions, including development, tissue damage response, and antiviral immunity. Here, we report the identification of a small molecule called (E)-*N*-(4-(*N*-(3-methoxypyrazin-2-yl)sulfamoyl) phenyl)-3-(5-nitrothiophene-2-yl)acrylamide—hereafter referred to as necrosulfonamide—that specifically blocks necrosis downstream of RIP3 activation. An affinity probe derived from necrosulfonamide and coimmunoprecipitation using anti-RIP3 antibodies both identified the mixed lineage kinase domain-like protein (MLKL) as the interacting target. MLKL was phosphorylated by RIP3 at the threonine 357 and serine 358 residues, and these phosphorylation events were critical for necrosis. Treating cells with necrosulfonamide or knocking down MLKL expression arrested necrosis at a specific step at which RIP3 formed discrete punctae in cells. These findings implicate MLKL as a key mediator of necrosis signaling downstream of the kinase RIP3.

INTRODUCTION

The importance of cell death in the life of metazoan animals has best been illustrated by the discovery that cell death is programmed and is executed by sophisticated cellular biochemical pathways (Ellis et al., 1991; Kerr et al., 1972; Li et al., 1997; Scaffidi et al., 1998).

Two well-characterized cell death pathways lead to the activation of caspase-3 and caspase-7, a pair of related executioner proteases that are responsible for the morphologically distinct form of cell death known as apoptosis (Thornberry and Lazebnik, 1998). One pathway, known as the intrinsic pathway, is initiated through mitochondria; the other is initiated through cell surface death receptors of the tumor necrosis factor (TNF) family of cytokines and is therefore referred to as the extrinsic pathway. The mitochondrial pathway is triggered by the proapoptotic members of the Bcl-2 family of proteins that render the outer membrane of mitochondria permeable to factors normally located within the intermembrane space, in particular cytochrome *c* and Smac/Diablo (Wang and Youle, 2009). The released cytochrome *c* binds to Apaf-1 protein to form a caspase-9 activating protein complex that cleaves and activates caspase-3/7 (Li et al., 1997). Smac/Diablo removes the inhibition of caspases imposed by the X-linked Inhibitor of Apoptotic Protein (XIAP) and induces cIAP1 and cIAP2 degradation (Du et al., 2000; Li et al., 1997; Verhagen et al., 2000; Yang and Du, 2004). The death receptors are activated after they have been occupied by their corresponding ligands. This leads to the formation of a death-inducing signaling complex (DISC), within which caspase-8, another upstream caspase of caspase-3 and -7, is activated (Ashkenazi and Dixit, 1999).

As important as caspase activity is for apoptosis, inhibiting caspases often delays but does not prevent cell death in mammalian cells if the death is through the mitochondrial pathway (Kroemer and Martin, 2005). In contrast, apoptosis resulting from activation of death receptors can be completely rescued by caspase inhibitors such as z-VAD-fmk. However, in some cell types, the same caspase inhibitor exacerbates cell death by switching on the necrotic cell death program (Cauwels et al., 2003; He et al., 2009; Vercammen et al., 1998).

The determining factor for the necrotic response is the receptor-interacting serine-threonine kinase 3 (RIP3, also known as RIPK3). Cells expressing RIP3 are capable of undergoing necrosis in response to the TNF family of cytokines (Cho et al., 2009; He et al., 2009; Zhang et al., 2009). These cells include mouse fibroblast L929 cells (in which TNF-induced necrosis was first observed), cells from the hematopoietic system, and epithelial cells of the gastrointestinal tract. During the necrosis induction process, RIP3 binds to the kinase RIP1 (which is also called RIPK1) through their respective RIP homotypic interaction motif (RHIM) domains. Inhibition of the kinase activity of RIP1 by the chemical inhibitor necrostatin-1 prevents the RIP1/RIP3 interaction and blocks necrosis (Degterev et al., 2008; He et al., 2009). Importantly, caspase-8 is able to cleave RIP1 and

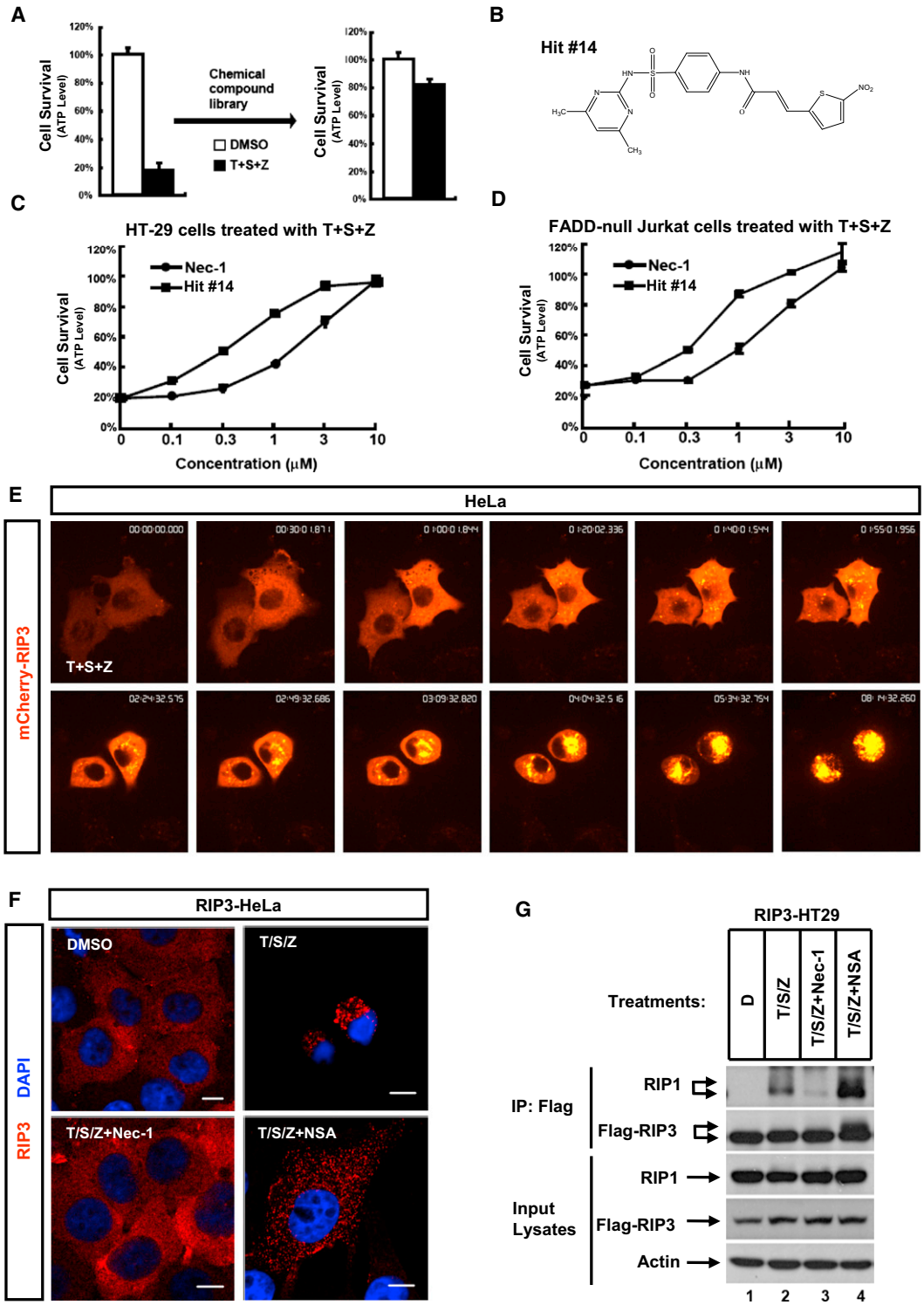

Figure 1. Necrosulfonamide Blocks Necrosis Downstream of RIP3 Activation

(A) Screen assay design as described in Experimental Procedures. The number of surviving cells was normalized to control cells that were treated with DMSO. Necrosis was induced by adding the final concentrations of 20 ng/ml TNF-α (T), 100 nM Smac mimetic (S), and 20 μM z-VAD (Z) to the cell culture wells. Identical concentrations of these necrosis-inducing agents were used in subsequent experiments unless otherwise stated. Necrostatin-1 (Nec-1) was used as a positive control for screening the necrosis inhibitors. The data are represented as the mean ± SD of duplicate wells.

(B) Chemical structure of the original hit compound (E)-*N*-(4-(*N*-(4,6-dimethylpyrimidin-2-yl)sulfamoyl)phenyl)-3-(5-nitrothiophene-2-yl)acrylamide, an analog of necrosulfonamide.

RIP3, effectively terminating necrosis (Feng et al., 2007; Lin et al., 1999). Thus, for necrosis to ensue, the inhibitory effect of caspase-8 must be overcome either by caspase inhibitors or by a substantial elevation of RIP3 levels, as occurs during tissue damage (He et al., 2009; Trichonas et al., 2010).

The importance of necrotic cell death has been illustrated by several recent findings. Breeding onto a RIP3 knockout background rescues the developmental defects of caspase-8 knockout mice. This indicates that the cardiac, vascular, and hematopoietic defects that occur during the development of caspase-8 knockout mice are caused by RIP3-mediated necrosis, unleashed by disrupting caspase-8 expression (Kaiser et al., 2011; Oberst et al., 2011). During viral infection, a lack of RIP3 allows for more rapid viral replication of both vaccinia virus and murine cytomegalovirus in mice (Cho et al., 2009; Upton et al., 2010). Moreover, RIP3 is markedly elevated in tissue damage models such as acute pancreatitis and retinal detachment (He et al., 2009; Trichonas et al., 2010). Abolishing RIP3 expression effectively reduces the degree of tissue damage, suggesting that RIP3-mediated necrotic death may exacerbate damage-induced inflammation, thereby aggravating the injury. Thus, a better understanding of the molecular pathway responsible for RIP3-mediated necrosis and the development of inhibitors of this pathway could serve urgent medical needs.

The mechanism by which RIP3 causes programmed necrotic cell death is still poorly understood. Unlike caspase-3/7, whose specific cleavage of important cellular substrates gives rise to the morphological traits and biochemical markers of apoptosis, RIP3 could potentially initiate many cellular responses. RIP3 autophosphorylates itself and also phosphorylates its partner kinase, RIP1, within the RIP1/RIP3 complex that is called necrosome (Declercq et al., 2009). However, the functional significance of these phosphorylation events and their downstream substrates are still unknown. Addressing these questions will likely be the key to deciphering the molecular pathway of necrosis.

We previously established a robust cell-based model of necrosis by treating human colon cancer HT-29 cells with a combination of TNF-α, a cell-permeable small molecule that mimics Smac function (Smac mimetic), and the pan-caspase inhibitor z-VAD-fmk (He et al., 2009; Li et al., 2004). Using this model, we screened ~200,000 chemical compounds for the ability to inhibit necrosis and found one compound that specifically blocked necrosis at a step downstream of RIP3 activation. A combination of chemical biology and biochemical approaches identified the biological target of the compound as the mixed lineage kinase domain-like protein (MLKL), which is a critical substrate of RIP3 during the induction of necrosis.

RESULTS

Identification of Necrosulfonamide as an Inhibitor of Necrosis Downstream of RIP3

Taking advantage of the robustness of the necrosis that is induced by combinatorial treatment with TNF-α, Smac mimetic, and z-VAD-fmk, we screened a chemical library of ~200,000 for compounds that blocked necrosis like necrostatin-1 (Figure 1A). One hit (Hit #14) that drew our attention was the compound (E)-*N*-(4-(*N*-(4,6-dimethylpyrimidin-2-yl)sulfamoyl)phenyl)-3-(5-nitrothiophene-2-yl)acrylamide shown in Figure 1B. The #14 compound blocked necrosis in both human colon cancer HT-29 cells and FADD null human T cell leukemia Jurkat cells with an IC_{50} less than 1 μM, which is more potent than necrostatin-1 (Figures 1C and 1D). Using a medicinal chemistry approach, we further identified a 3-methoxypyrazin-2-yl derivative of the original hit as the most efficacious analog in this class of compounds, with an IC_{50} of less than 0.2 μM (Figure S1A available online). This compound will hereafter be referred to as necrosulfonamide (NSA). Notably, necrosulfonamide had no effect on apoptosis induced by TNF-α plus Smac mimetic in non-RIP3-expressing Panc-1 cells, even at 5 μM concentration (Figure S1B).

Because FADD null Jurkat cells cannot activate caspase-8 in response to extrinsic apoptosis signals and therefore undergo necrosis when treated with TNF-α alone, they were used to eliminate the possibility that necrosulfonamide blocks necrosis by interfering with the chemical activity of Smac mimetic or caspase-inhibitor z-VAD. Indeed, necrosis in FADD null cells induced by TNF-α alone was still efficiently blocked by necrosulfonamide similar to necrostatin-1 (Figure S1C). HeLa cells normally do not express RIP3 and are unable to respond to the necrosis stimulus. However, the necrosis response in HeLa cells can be reconstituted by ectopic expression of RIP3. Consistently, in a HeLa cell line in which RIP3 was expressed and caspase-8 was knocked down, necrosis-induced by TNF-α plus Smac mimetic (no need for z-VAD) was also efficiently blocked by necrosulfonamide (Figure S1D). Interestingly, in a mouse 3T3 cell line expressing mouse RIP3, necrosis induced by either TNF-α/z-VAD or TNF-α/Smac mimetic/z-VAD was totally insensitive to necrosulfonamide inhibition even though necrostatin-1 efficiently mitigated the cell death (Figure S1E). This observation gave us a critical clue in the effort to identify the functional cellular target of necrosulfonamide later on.

To explore how necrosulfonamide blocks necrosis, a series of live-cell images of a mCherry-RIP3 fusion protein in HeLa cells undergoing necrosis were taken. These images revealed that RIP3, which is usually uniformly diffused throughout the cytosol

(C and D) Dose-dependent inhibition of necrosis by the hit compound or necrostatin-1 (Nec-1) in HT-29 (C) and FADD null Jurkat cells (D). The cells were treated with T/S/Z plus the indicated concentrations of the hit compound and Nec-1. Cell viability was determined by measuring ATP levels. The data are represented as the mean ± SD of duplicate wells.

(E) Live-cell fluorescent images of mCherry-tagged RIP3 in HeLa cells treated with T/S/Z. The time after the treatment is indicated.

(F) The effects of necrostatin-1 and necrosulfonamide (NSA) on the formation of RIP3 punctae. RIP3-HeLa cells were treated with the indicated stimuli for 8 hr. The distribution of RIP3 (red) was detected by immunofluorescence as described in Experimental Procedures. The scale bars represent 10 μm.

(G) The effect of necrosulfonamide on the RIP1/RIP3 interaction. Flag-tagged RIP3-HT-29 cells were treated with the indicated stimuli for 6 hr. Then the cell extracts were prepared and used for immunoprecipitation with an anti-Flag antibody as described in Experimental Procedures. The immunocomplexes were then analyzed by western blotting using antibodies as indicated. Aliquots of 20 μg whole-cell lysates (Input) were subjected to SDS-PAGE. β-Actin is shown as a loading control. Immunoprecipitation, IP.

See also Figure S1.

of living cells, gradually formed discrete punctae that were enlarging as necrosis progressed (Figure 1E). The mCherry-RIP3 protein functioned similarly to native RIP3 because expressing the mCherry-RIP3 fusion protein in HeLa cells rendered them necrosis responsive (Figure S1F). In the presence of necrosulfonamide, the discrete RIP3 punctae were detected but failed to enlarge (Figure 1F), indicating that the compound blocked necrosis at a specific step in the necrosis pathway.

We then analyzed the immunocomplex obtained from a Flag-tagged RIP3 pull-down and found that, unlike necrostatin-1, necrosulfonamide did not block necrosis-induced RIP1 and RIP3 interactions (Figure 1G, lanes 3 and 4). Instead, the interaction between RIP1 and RIP3—and the upward shifts in their SDS-PAGE gel migration owing to their phosphorylation—was enhanced by necrosulfonamide (Figure 1G, lane 4). These results indicated that necrosulfonamide blocked necrosis at an unknown step downstream of RIP3 activation.

The Interaction of RIP3 with MLKL Is Enhanced by Necrosis Induction

We sought to identify proteins associated with RIP3 in cells treated with necrosis inducers in the presence of necrosulfonamide. As shown in Figure 2A, on an SDS-PAGE gel, a protein band that specifically appeared with the RIP3 immunocomplex under these conditions migrated just above the position of the IgG heavy chain. Mass spectrometry analysis identified this protein as the mixed lineage kinase-domain like protein (MLKL). MLKL contains a kinase-like domain and is most closely related to the mixed lineage kinases that function as MAPKKs in the JNK and p38 kinase activating pathways (Gallo and Johnson, 2002). However, unlike a bona fide kinase, the kinase-like domain of MLKL lacks a phosphate-binding glycine-rich P loop, and the key aspartate 349 residue that coordinates the magnesium ion in the kinase has changed to a glycine residue in MLKL. MLKL is therefore a kinase-dead protein.

To verify the specific association between RIP3 and MLKL in a different cell line, we used an anti-Flag antibody to immunoprecipitate Flag-tagged RIP3 that was expressed in HT-29 cells. RIP3 was phosphorylated, as indicated by the upward shift in the protein band under necrosis-inducing conditions (compare lane 1 with lanes 2 and 3 in Figure 2B). This shift was enhanced by necrosulfonamide, which is consistent with the notion that this compound blocks necrosis downstream of RIP3 kinase. MLKL was also shifted after necrosis was induced (Figure 2B, lanes 2 and 3). The MLKL/RIP3 complex was present in living cells, but the amount of MLKL that was associated with RIP3 increased upon necrosis induction (Figure 2B, compare lane 1 with lanes 2 and 3).

Knockdown of MLKL Blocks the Progression of Necrosis

To test its role in necrosis, we knocked down MLKL with four different siRNA oligos in HT-29 cells, human gastric cancer MKN45 cells, and in mouse L929 cells (Figure S2). All four siRNA oligos (targeting either human or mouse MLKL) knocked down MLKL to different degrees, and the knockdown efficiency correlated with the degree of necrosis inhibition (Figures S2A–S2F). To eliminate the possibility of off-target effects for these siRNA oligos, we introduced silent mutations into one of the oligo-targeting sites in human MLKL and performed the rescue experiment with this cDNA in RIP3-expressing HeLa cells. As shown in Figure 2C, knockdown of MLKL blocked TNF-α/Smac mimetic/z-VAD-fmk-induced necrosis. Transfection of the cDNA restored the necrosis response, whereas a control siRNA oligo targeting luciferase (luc) had no effect on necrosis.

We further analyzed the RIP1/RIP3 interaction by coimmunoprecipitation upon MLKL knockdown. As shown in Figure 2D, after necrosis induction, RIP3 associated with RIP1, and its mobility shifted regardless of the presence of MLKL (lanes 2 and 3 and 5 and 6). Interestingly, as seen with necrosulfonamide treatment, MLKL knockdown enhanced RIP1/RIP3 interactions (Figure 2D, compare lanes 2 and 5). However, this interaction was not further enhanced by necrosulfonamide treatment after MLKL knockdown (Figure 2D, compare lane 3 with lane 6). These data suggest that the knockdown of MLKL and necrosulfonamide treatment have a similar effect on RIP1/RIP3 interactions.

Necrosulfonamide Targets MLKL

Because treating necrotic cells with necrosulfonamide arrests necrosis at a step at which RIP3 forms discrete punctae within the cytosol, we performed a similar analysis of RIP3 distribution during necrosis after MLKL knockdown using immunofluorescent staining. As shown in Figure 3A, knocking down MLKL also arrested cellular necrosis at this step (Figure 3Af). Further treatment with necrosulfonamide did not change the RIP3 distribution pattern, which indicates that knocking down MLKL has the same effect on necrosis as necrosulfonamide treatment (Figures 3Ac and 3Ag). In contrast, treatment with necrostatin-1 prevented the formation of RIP3 punctae, regardless of MLKL expression status (Figures 3Ad and 3Ah).

To test whether MLKL is the direct cellular target of necrosulfonamide, we added a biotin tag to the compound by chemical synthesis and precipitated the interacting protein with streptavidin-conjugated beads. To enhance the capacity of the affinity purification process and to allow for the isolation of low-abundance or low-affinity proteins, a polyproline-rod spacer was inserted between the biotin tag and the compound (Figure 3B) (Sato et al., 2007). This biotinylated necrosulfonamide (biotin-NSA) retained its ability to block necrosis, although it had to do so with ~10-fold higher concentration (Figure S3A). When the biotin-NSA was incubated with cell extracts prepared from the RIP3-expressing HeLa cells and pulled down with streptavidin-conjugated beads, the pellet contained endogenous MLKL as well as the RIP3 transgene product (Figure 3C, lane 2). The non-biotin-labeled necrosulfonamide efficiently competed off MLKL and RIP3 binding to the beads (Figure 3C, lane 1). The specificity of the MLKL pull-down was further confirmed using siRNA knockdown of MLKL (Figure 3C, lanes 3 and 4). We also used the biotin-NSA to study endogenous MLKL and RIP3 interaction in HT-29 cells. As shown in Figure S3B, endogenous RIP3 was also pulled down with MLKL before necrosis induction, confirming the observation that there was a basal level of MLKL/RIP3 interaction in living cells (Figures 2B and 2D). As necrosis progressed, MLKL and RIP3 interaction became more robust as shown by RIP3 antibody pull-down (Figures 2B and 2D). At the same time, less MLKL/RIP3 bound to the

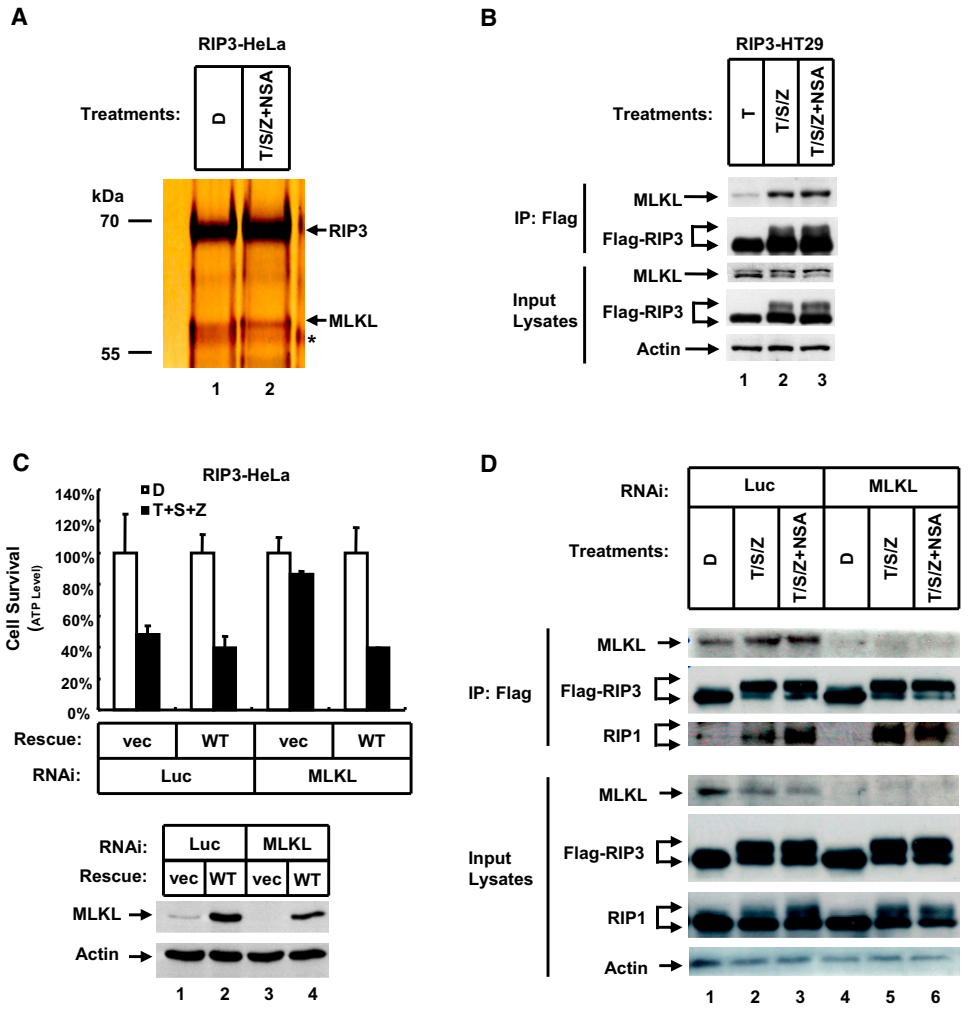

Figure 2. MLKL Is Required for TNF-α-Induced Necrosis

(A) Identification of MLKL as a necrosome component. RIP3-HeLa cells (RIP3 was double tagged with Flag and HA) were treated as indicated. The cells were then harvested, and whole-cell extracts were sequentially immunoprecipitated with anti-Flag and anti-HA antibodies as described in Experimental Procedures. The peptide-eluted RIP3-associated complexes were then analyzed by SDS-PAGE followed by silver staining. The indicated bands were excised and subjected to mass spectrometry analysis. The asterisk (*) denotes the IgG heavy chain.

(B) The MLKL-RIP3 interaction is enhanced following necrosis induction. Flag-tagged RIP3-HT-29 cells were treated with the indicated stimuli for 6 hr. The cells were then harvested, and the whole-cell extracts were immunoprecipitated with anti-Flag antibody as described in Experimental Procedures. The immunocomplexes were analyzed by western blot analysis using the indicated antibodies. Aliquots of 20 μg whole-cell lysates (Input) were subjected to SDS-PAGE followed by western blot analysis of RIP1, RIP3, and MLKL. β-Actin is shown as a loading control.

(C) Rescue of the MLKL knockdown phenotype by an siRNA-resistant MLKL. MLKL was knocked down in RIP3-HeLa cells and rescued with an siRNA-resistant MLKL-expressing construct as indicated. Cell viability was determined by measuring cellular ATP levels (upper panel). The data are represented as the mean ± SD of duplicate wells. The MLKL levels were measured by western blotting (lower panel). Luc, luciferase siRNA control; vec, vector control; WT ,WT MLKL.

(D) The effect of MLKL on the RIP1-RIP3 complex. MLKL in RIP3-HeLa cells was knocked down as in (C) followed by treatment with DMSO (D), or T/S/Z, or T/S/Z plus necrosulfonamide as indicated for 6 hr. The RIP1-RIP3 complex was immunoprecipitated with an anti-Flag antibody. The immunocomplexes were analyzed by western blotting using antibodies as indicated.

See also Figure S2.

biotin-NSA/streptavidin-conjugated beads (Figure S3B). These results suggested that the binding site on MLKL for necrosulfonamide became nonaccessible once RIP1/RIP3/MLKL necrosome formed.

Structure-activity relationship (SAR) studies of necrosulfonamide identified several important functional groups whose structural modifications abolished the molecule's activity (Figures S4A and S4B). These inactive derivatives of necrosulfonamide did not compete with the biotin-labeled necrosulfonamide for MLKL binding (Figure S4C).

To pinpoint which part of MLKL binds to necrosulfonamide, we separately expressed the N-terminal 178 amino acid residues of MLKL and the C-terminal kinase-like (residue 179-471) region in HeLa cells (Figure 3D, lanes 5 and 6). Although the C-terminal

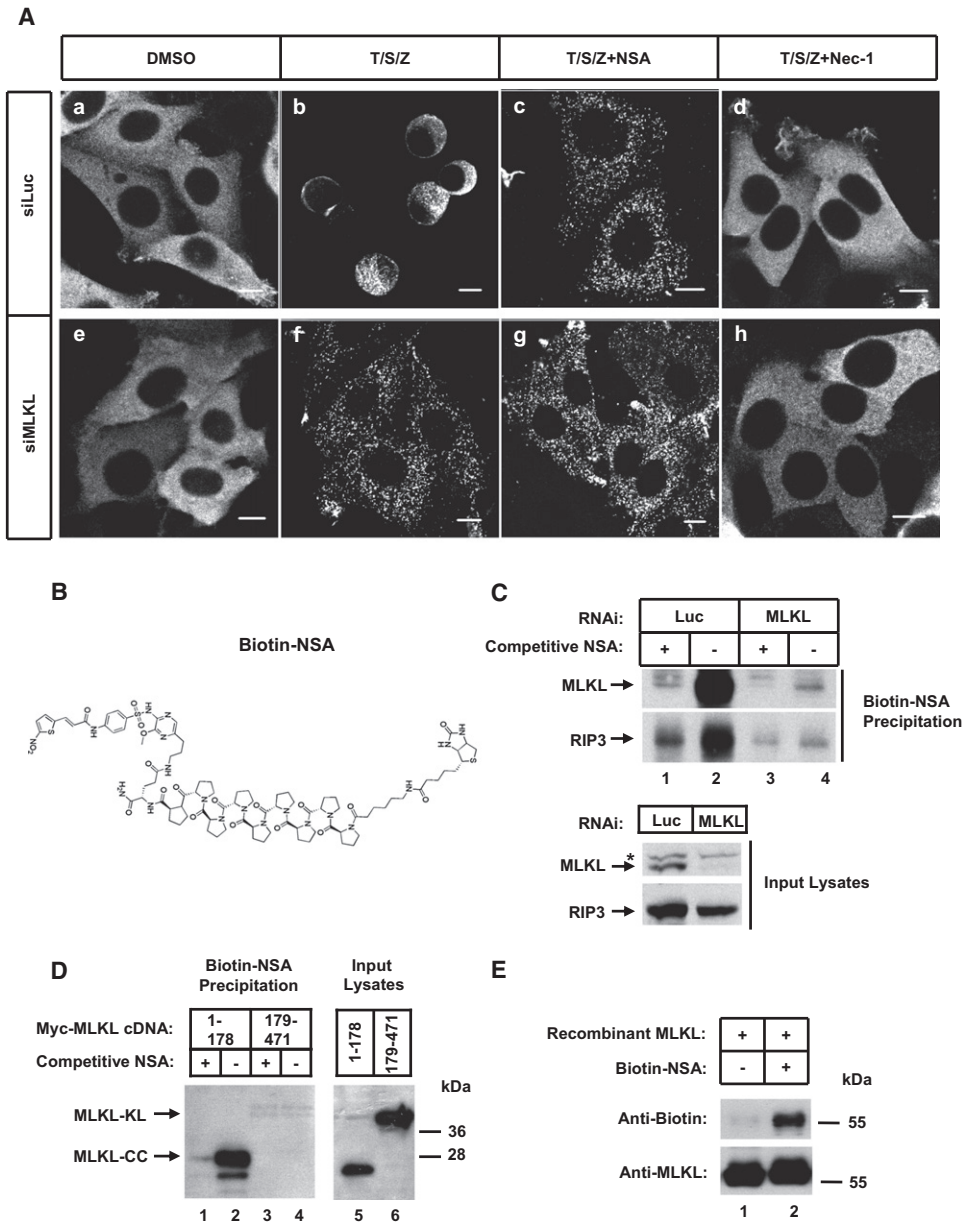

Figure 3. Identification of Cellular Targets of Necrosulfonamide

(A) RIP3-HeLa cells were transfected with siRNA either targeting MLKL or luc as indicated. After 48 hr, each well of cells was treated as indicated for 8 hr (a–h). The distribution of Flag-RIP3 was detected by immunofluorescence using an anti-Flag antibody followed by a fluorescein-conjugated secondary antibody as described in Experimental Procedures. The scale bars represent 10 μm.

(B) The chemical structure of biotin-NSA. The compound was synthesized as described in Experimental Procedures.

(C) Identification of MLKL as the cellular target of necrosulfonamide. RIP3-HeLa cells were transfected with siRNA targeting either MLKL or luc as a control. After 48 hr, the cells were harvested, and cell lysates were used for biotin-NSA pull-down as described in Experimental Procedures. Aliquots of 20 μg of whole-cell lysates were subjected to western blot analysis to measure the input RIP3 and MLKL levels. The asterisk (*) denotes a cross-reacting band that was present in the input lysates.

(D) Necrosulfonamide targets the CC domain of MLKL (MLKL-CC). The indicated fragments of MLKL with an N-terminal myc tag were expressed in HeLa cells and collected from the cell extracts with biotin-NSA plus streptavidin-conjugated beads. The proteins bound to the beads were analyzed by western blot analysis using an anti-Myc antibody. Aliquots of 20 μg of whole-cell lysates were subjected to western blot analysis to measure the input MLKL levels. MLKL-KL, kinase-like domain of MLKL.

(E) Necrosulfonamide interacts with MLKL through covalent bonding. Recombinant MLKL was generated as described in Experimental Procedures. Aliquots of 1 μg of MLKL were incubated with 2 nmol biotin-NSA at 4°C. After 6 hr, the protein samples were subjected to SDS-PAGE followed by western blotting analysis using an anti-biotin antibody. An equal aliquot of input MLKL was measured by western blot analysis.

See also Figure S3.

kinase-like region was expressed at a slightly higher level, only the N-terminal fragment of MLKL was pulled down by the biotinylated compound (Figure 3D, lane 2).

The SAR studies of necrosulfonamide revealed that its α,β-unsaturated enone moiety is required for its biological activity (Figures S4A and S4B, NSA-D1), suggesting that it serves as a Michael acceptor that covalently binds to its target. To test this idea, we incubated the biotinylated compound with recombinant MLKL and probed the biotin signal after resolving the reaction mixture on SDS-PAGE. As shown in Figure 3E, a biotin signal was readily detected at the position of recombinant MLKL (lane 2).

Necrosulfonamide Targets the Cys86 Residue of MLKL

Although MLKL is important for necrosis in mouse L929 fibrosarcoma cells (Figure S2E), treatment of L929 or mouse RIP3-expressing 3T3 cells with necrosulfonamide at more than 10-fold higher concentrations than what was used to inhibit necrosis in human cells did not rescue necrosis (Figures 4A and S1E). Consistent with this result, the biotinylated compound did not precipitate mouse MLKL, even though it was ectopically expressed in human cells at a similar level as its human counterpart, and a significant amount of human MLKL was precipitated under the same conditions (Figure 4B, compare lanes 1 and 2 to lanes 3 and 4). These experiments showed that the compound targets human MLKL, but not mouse MLKL.

Given that the compound binds within the N-terminal 178 residues of human MLKL and covalently modifies MLKL through Michael addition at a reactive amino acid residue most likely to be a cysteine, we examined this region of human and mouse MLKL for differences in their cysteine residues (Figure 4C). All of the cysteine residues within this region are conserved between the human and mouse homologs of MLKL, with the single exception of a cysteine at position 86 in human MLKL that corresponds to a tryptophan residue in the mouse homolog. Mutating this cysteine into a serine (the C86S mutant) completely abolished the compound's ability to bind to human MLKL (Figure 4D, compare lanes 1 and 2 to lanes 3 and 4). Consistent with this finding, expressing the C86S mutant siRNA-resistant version of human MLKL rendered cells insensitive to necrosulfonamide treatment, although the mutant MLKL retained the ability to reconstitute necrosis after endogenous MLKL was knocked down (Figures 4E and 4F). In contrast, wild-type (WT) MLKL restored both necrosis and necrosulfonamide sensitivity under the same condition (Figures 4E and 4F).

MLKL Is Phosphorylated by RIP3 in Response to Necrosis Induction

MLKL consists of an N-terminal coiled-coil (CC) domain and a C-terminal kinase-like domain. RIP3 has an N-terminal kinase domain that is followed by an RHIM domain, through which it interacts with RIP1 (Figure 5A). To study the interaction between MLKL and RIP3, we coexpressed myc-tagged MLKL and Flag-tagged full-length RIP3 or its kinase domain only in HeLa cells. As shown in Figure 5B, both full-length RIP3 and the RIP3 kinase domain coimmunoprecipitated with MLKL, indicating that the kinase domain is sufficient to bind MLKL (Figure 5B, lanes 4–6). Interestingly, when the kinase domain of RIP3 was coexpressed with MLKL, a doublet of bands appeared, and only the upper band was coprecipitated with MLKL (Figure 5B, lanes 2 and 5). When the reciprocal experiment was performed with the RIP3 kinase domain, only full-length MLKL and its kinase-like domain, but not its CC domain, were coimmunoprecipitated, indicating that the binding of MLKL to RIP3 occurs through MLKL's kinase-like domain (Figure 5C, lanes 4–6). Consistently, when the RIP3 kinase domain was coexpressed with the kinase-like domain of MLKL, a shifted band (most likely a result of autophosphorylation) was observed (Figure 5C, lanes 3 and 6). These data suggested that the association between the RIP3 kinase domain and the MLKL kinase-like domain facilitated RIP3 autophosphorylation, resulting in an evident upward shift of its protein band.

Because RIP3 binds MLKL at its kinase domain, we tested whether the kinase activity of RIP3 was required for their interaction. As shown in Figure 5D, ectopically expressed WT RIP3 bound to MLKL in HeLa cells, regardless of necrosis induction; however, RIP3 mobility shift was more apparent under necrotic conditions (Figure 5D, lane 2). A kinase-dead form of RIP3 (K50A) was unable to bind MLKL even though it was expressed at a similar level of WT protein (Figure 5D, lanes 3 and 4). An identical result was obtained with another kinase-dead mutant of RIP3 (see below).

To test whether RIP3 can directly phosphorylate MLKL, we performed an in vitro kinase assay using RIP1 and RIP3 immunopurified from the HeLa cells in which they were ectopically expressed. As shown in Figure 5E, both RIP1 and RIP3 phosphorylated a nonspecific substrate protein, Myelin basic protein (MBP), when they were incubated together in vitro (lanes 2 and 5), whereas MLKL was only phosphorylated by RIP3 (lane 6).

Consistent with the protein-binding data, the kinase-like domain of MLKL was phosphorylated when incubated with RIP3 in the in vitro phosphorylation assay. In contrast, the N-terminal CC domain of MLKL was not phosphorylated (Figure 6A, lanes 5–7).

To precisely map the RIP3 phosphorylation site on MLKL, we coimmunoprecipitated MLKL with an anti-RIP3 antibody under the necrosis-inducing conditions and subjected the immunocomplex to SDS-PAGE. The protein band that corresponded to MLKL was excised from the gel and digested with trypsin. The digested peptides were then analyzed by mass spectrometry. After a protein database search, one double-phosphorylated peptide with the sequence $KTQ_pT_pSMSLGTTR$ was identified. Tandem mass spectrometry of this peptide unambiguously identified threonine 357 and serine 358 as being phosphorylated (Figure S5A).

To verify the functional significance of these phosphorylation events on MLKL, we introduced single and double mutations at T357 and S358 into the template of the siRNA-resistant cDNA of MLKL. These constructs were then transfected into RIP3-expressing HeLa cells after knockdown of endogenous MLKL by the siRNA. As shown in Figure 6B, WT MLKL reconstituted the necrosis response, whereas the empty vector did not. Interestingly, the T357A/S358A double mutant was unable to reconstitute necrosis, even though it was expressed at WT level. The single mutant protein of either T357A or S358A behaved

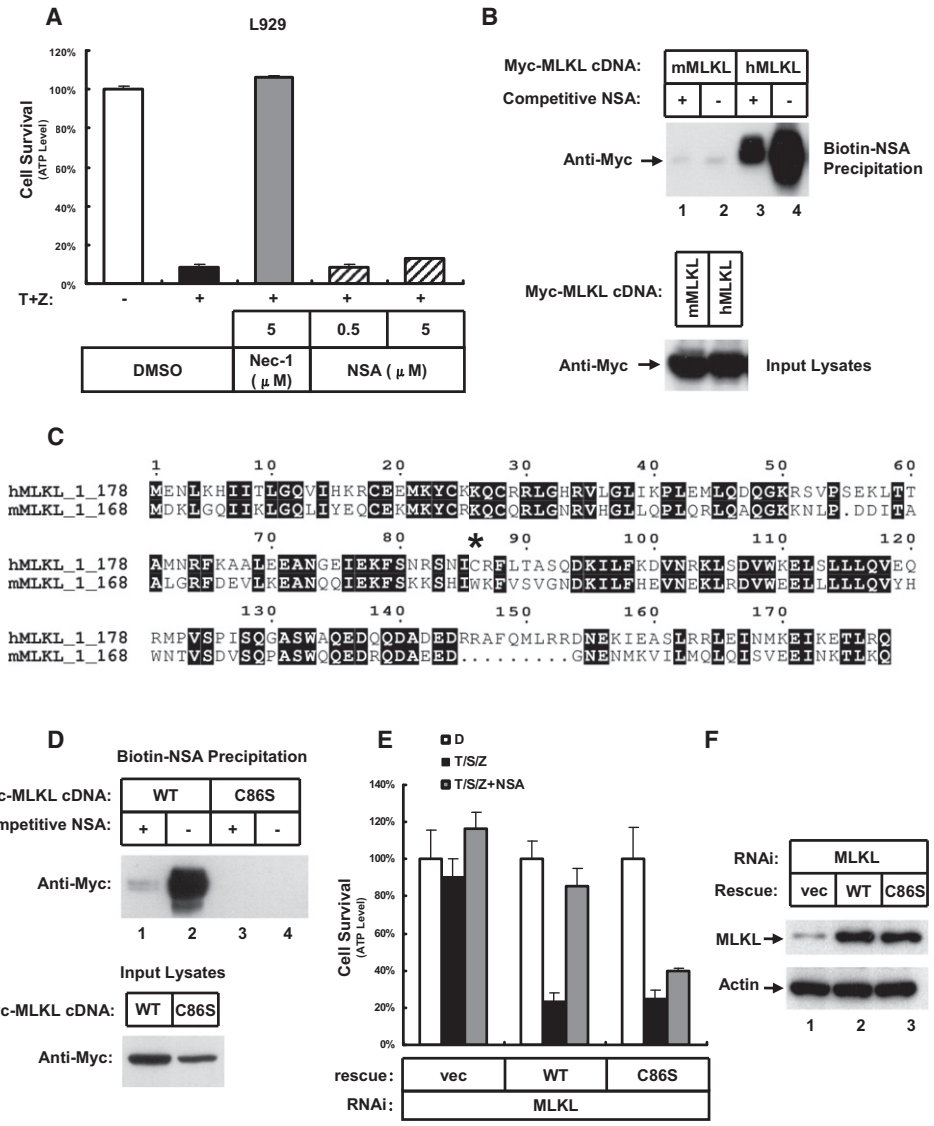

Figure 4. Identification of Cys86 of MLKL as the Necrosulfonamide-Binding Residue

(A) Mouse fibrosarcoma L929 cells were treated as indicated for 24 hr. Cell viability was determined by measuring ATP levels. The data are represented as the mean ± SD of duplicate wells.

(B) Biotin-NSA pull-down analysis of human MLKL and mouse MLKL. Aliquots (1 mg) of whole-cell lysates from HeLa cells transfected with myc-tagged mouse or human MLKL were used for biotin-NSA precipitation as described in Experimental Procedures. Aliquots of 20 μg whole-cell lysates were subjected to western blot analysis to measure the input mouse and human MLKL levels.

(C) Alignment of the CC domain of human and mouse MLKL. Identical amino acid residues in the sequences are shaded. The asterisk (*) denotes cysteine 86 (Cys86) in human MLKL, which corresponds to a tryptophan in mouse MLKL.

(D) Mutation analysis of the necrosulfonamide-targeting site. An aliquot (1 mg) of whole-cell lysate from HeLa cells transfected with Myc-tagged WT MLKL or the C86S mutant was used for a biotin-NSA pull-down assay as in (B). Aliquots of 20 μg whole-cell lysates were subjected to western blot analysis to measure the input MLKL levels.

(E) Cys86 mutant MLKL confers necrosulfonamide resistance. The knockdown and rescue experiments for MLKL were performed in RIP3-HeLa cells as in Figure 2C. After necrosis induction as indicated, cell viability was determined by measuring ATP levels. The data are represented as the mean ± SD of duplicate wells.

(F) The MLKL levels in knockdown and rescue experiments were measured by western blot analysis.

See also Figure S4.

similarly to the WT protein, indicating that phosphorylation at either of these positions was sufficient for necrosis (Figure S5B).

We also generated purified recombinant MLKL bearing mutations at both T357 and S358 and used similar amounts of WT and mutant MLKL in an in vitro kinase assay. In contrast to WT MLKL

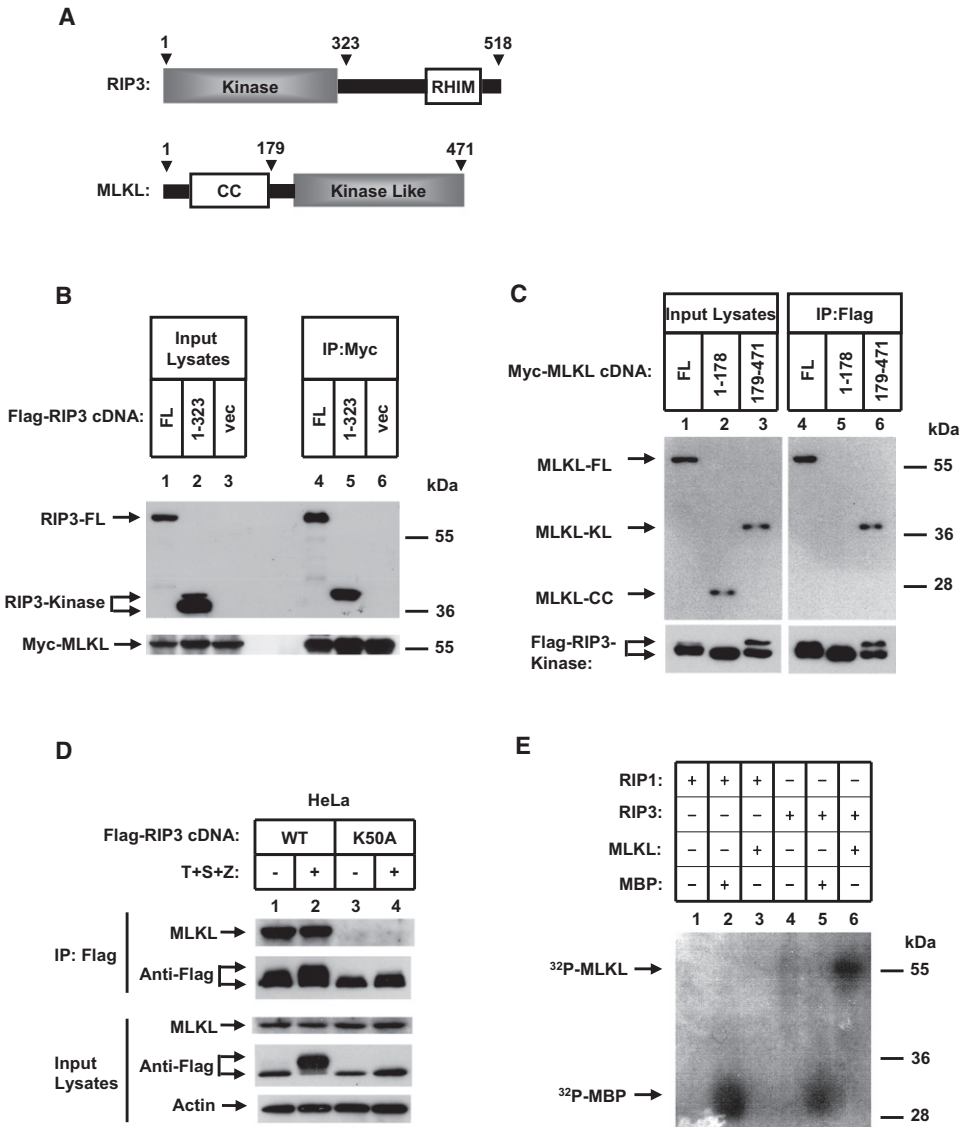

Figure 5. MLKL Binding to RIP3 Depends on the Kinase Activity of RIP3

(A) Domain structures of RIP3 and MLKL.

(B) Mapping the MLKL-binding domain in RIP3. Full-length and truncated RIP3 was cotransfected with Myc-tagged MLKL in HeLa cells for 24 hr. Then, 1 mg aliquots of whole-cell lysates were used for immunoprecipitation with an anti-Myc antibody. The immunocomplexes of MLKL (IP:Myc) were analyzed by western blot analysis using an anti-Flag antibody for RIP3 (lanes 4–6). Aliquots of 20 μg whole-cell lysates were also subjected to western blotting analysis to measure the expression of RIP3 (lanes 1–3). RIP3-kinase, kinase domain of RIP3; RIP3-FL, full-length RIP3.

(C) Mapping the RIP3-binding domain in MLKL. Full-length and truncated MLKL was cotransfected with Flag-tagged kinase domain of RIP3 in HeLa cells for 24 hr. Then, 1 mg aliquots of whole-cell lysates were used for immunoprecipitation with an anti-Flag antibody, and the immunocomplexes were analyzed by western blot analysis using an anti-Myc antibody (lanes 4–6). Aliquots of 20 μg whole-cell lysates were subjected to western blot analysis to measure the transfection efficiencies (Input Lysates, lanes 1–3). MLKL-FL, full-length MLKL; MLKL-CC, CC domain of MLKL; MLKL-KL, kinase-like domain of MLKL.

(D) Coprecipitation of MLKL with WT and kinase-dead mutant RIP3. Flag-tagged WT or the kinase-dead (K50A) mutant RIP3 was transfected in HeLa cells. After 24 hr, the cells were treated as indicated for 6 hr. RIP3 was immunoprecipitated from 1 mg cell lysate with an anti-Flag antibody and analyzed by western blot analysis using an anti-MLKL antibody. Aliquots of 20 μg whole-cell lysates were subjected to western blot analysis to measure the levels of RIP3 and MLKL (Input Lysates). β-Actin was shown as a loading control.

(E) In vitro kinase assay. RIP1 and RIP3 were immunopurified and used in a kinase assay with [^{32}P]γ-ATP and the purified recombinant MLKL as described in Experimental Procedures. The same amount of MBP was also included as an artificial substrate to normalize the kinase enzymatic activity of RIP1 and RIP3. See also Figure S6.

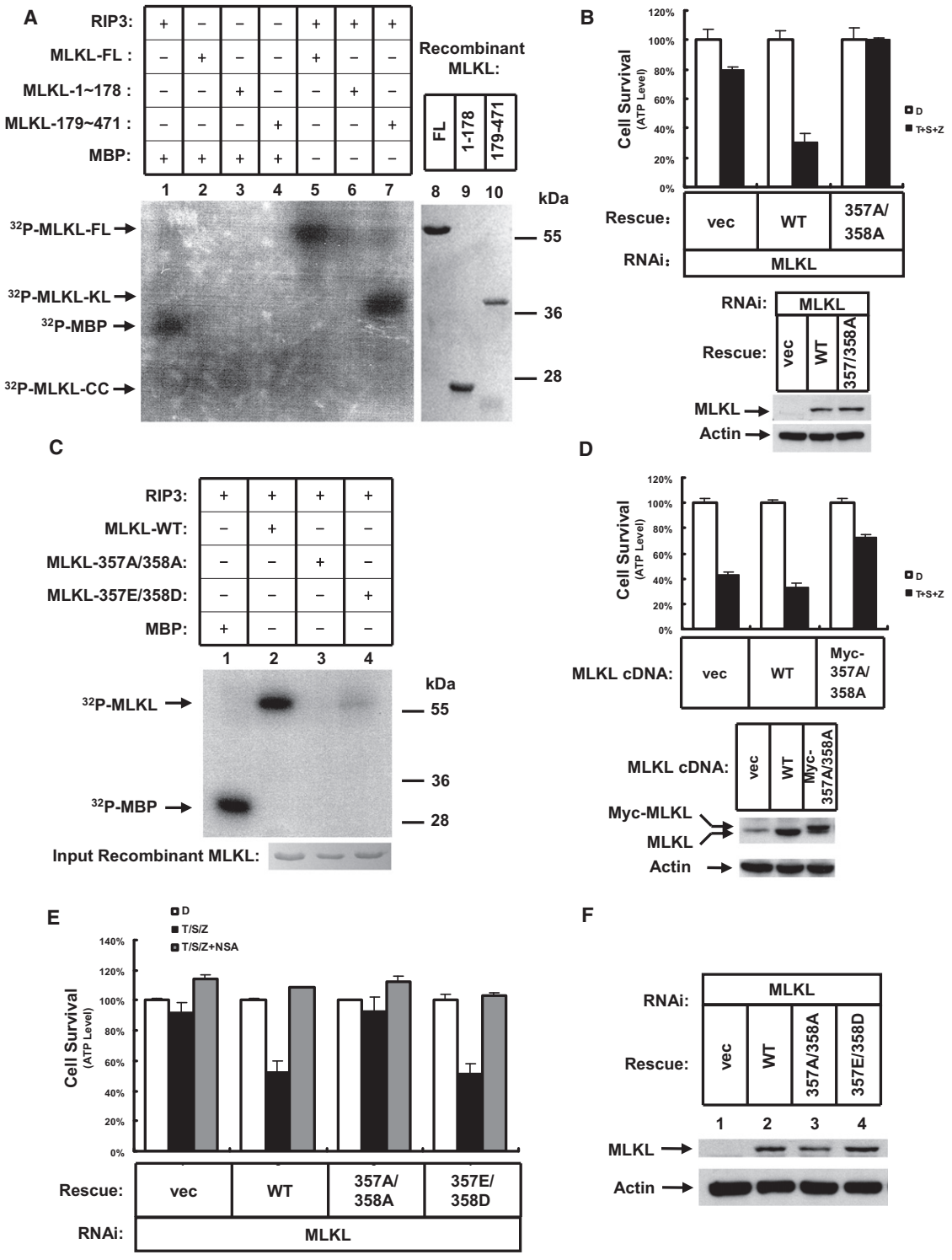

Figure 6. Characterization of the Phosphorylation Sites on MLKL

(A) Deletion analysis of the phosphorylation domain on MLKL by in vitro kinase assay. RIP3 was purified and used in a kinase assay as in Figure 5E by incubating with [^{32}P]γ-ATP and the purified deletion mutants of MLKL (lanes 1–7). The right panel shows the Coomassie blue staining of purified input MLKL (lanes 8–10). MLKL-FL, full-length MLKL; MLKL-CC, CC domain of MLKL; MLKL-KL, kinase-like domain of MLKL.

(B) A phosphorylation site mutant of MLKL fails to rescue necrosis in MLKL knockdown cells. Knockdown and rescue experiments on RIP3-HeLa cells were performed as in Figure 2C. The data are presented as the mean ± SD of duplicate wells. The MLKL levels in knockdown and rescue experiments were measured by western blot analysis as shown in the bottom panel.

(Figure 6C, lane 2), neither the T357A/S358A mutant nor the phosphomimetic mutant of MLKL (T357E/S358D) was phosphorylated by RIP3 (Figure 6C, lanes 2–4).

The T357A/S358A MLKL double mutant retained its ability to bind RIP3 (Figure S5D), raising the possibility that it might block necrosis in a dominant-negative manner. Indeed, when this mutant MLKL was expressed in HeLa cells without knocking down endogenous MLKL, necrosis was still attenuated (Figure 6D), whereas similar amount of WT MLKL enhanced necrosis.

We also tested if the T357E/S358D phosphomimetic MLKL retained the ability to induce necrosis. As shown in Figures 6E and 6F, this mutant restored both the necrosis response and sensitivity to necrosulfonamide, indicating that the inhibitory effect of necrosulfonamide cannot be bypassed by phosphorylation of these two sites. Both the phosphorylation site mutant and phosphomimetic versions of MLKL were still able to bind to necrosulfonamide (Figure S5E).

The T357 and S358 sites in human MLKL are conserved in rat, bovine, and chimpanzee. In mouse, the corresponding threonine 357 has changed to an asparagine, but the serine 358 is conserved (Figure S5C). Mouse RIP3 only binds to mouse MLKL, but not the human homolog (Figure S6).

Phosphorylation of Human RIP3 at Serine 227 Is Required for Binding MLKL

Although RIP3 is highly phosphorylated upon necrosis induction, the functional significance of these modifications has not been characterized. The data shown in Figure 5B suggested that the phosphorylation of RIP3 kinase domain was required for MLKL binding. To quantitatively characterize RIP3 phosphorylation during necrosis, we performed a stable isotope labeling of amino acids in cell culture (SILAC) experiment. RIP3 was immunoprecipitated from the heavy isotope (^{13}C, ^{15}N)-labeled cells after necrosis induction with TNF-α/Smac mimetic/z-VAD and then mixed with RIP3 from the non-necrotic (nonlabeled cells). As shown in Figure 7A, mass spectrometric analysis of these immunoprecipitated proteins identified a pair of light and heavy isotope-labeled peptides that matched a single-phosphorylated RIP3 peptide. The heavy/light peptide ratio was calculated as 8.95 using the extracted ion chromatogram (XIC) of this peptide pair, indicating that the phosphorylation level of this peptide was greatly enhanced upon necrosis induction. The heavy isotope-labeled phosphorylated peptide was then subjected to direct sequencing by tandem mass spectrometry, which identified this monophosphorylated peptide as EVELPTEP$_p$SLVYEAVCNR, with S227 as the phosphorylated amino acid residue (Figure 7B). Importantly, the phosphorylation site mutant (S227A) lost its ability to bind MLKL, similar to another kinase-dead mutant of RIP3 (D142N) (Figure 7C).

Consistent with this binding result, RIP3 protein bearing the single S227A mutation was unable to reconstitute necrosis in HeLa cells and behaved like the kinase-dead mutant (D142N) (Figure 7D).

The phosphorylation site of S227 is conserved among human, rat, chimpanzee, and mouse. Additionally, a mutation of the corresponding site of mouse RIP3 (S232A) also abolished its ability to reconstitute necrosis in NIH 3T3 cells (Figure S7).

DISCUSSION

MLKL Is a Core Component of the RIP1/RIP3 Necrosome

The aforementioned experimental results revealed that MLKL is one of the core components of the necrosis-inducing signaling complex called the necrosome, which also contains RIP1 and RIP3 (Declercq et al., 2009). MLKL does not possess intrinsic kinase activity, owing to its lack of a phosphate-binding P loop and the replacement of a key amino acid residue that is required for kinase activity. However, its binding to RIP3 through the kinase-like domain is critical for necrosis to proceed. Without MLKL, the necrosome was arrested in a precursor form, and RIP3-containing complexes manifested as smaller, uniformly distributed cytoplasmic punctae.

As illustrated in Figure 7E, MLKL seems to have a basal level of association with RIP3. Nevertheless, the interaction between MLKL and RIP3 is augmented during the necrosome initiation induced by TNF-α-mediated RIP1 activation. The enhanced interaction could be due to increased RIP3 kinase activity and its subsequent autophosphorylation at residue S227, which is required to form a stable complex with MLKL.

Another key phosphorylation event is the dual phosphorylation of T357 and S358 on MLKL, a likely marker for necrosome activation. These phosphorylated residues seem to have a redundant function because only the double phosphorylation site mutant was able to abolish MLKL function, and a single mutation at either of these sites still rescued necrosis. This finding may explain the observation that in mouse MLKL, only the S358 site is conserved and, thus, may be sufficient in transducing necrosis signal in mouse cells. The two phosphorylation sites on human MLKL are located within the protein's kinase domain-like activation loop. Although not essential for MLKL binding, phosphorylation of these two sites may expose its kinase domain, thus allowing the protein to interact with its downstream effectors, which leads to higher levels of organization that are observed in the late stages of necrosis progression.

(C) In vitro kinase assay analysis of WT and phosphorylation site mutant MLKL. RIP3 was purified and used in in vitro kinase assay as in Figure 5E by incubating with [^{32}P]γ-ATP and purified recombinant MLKL (lanes 1–4). The bottom panel shows the Coomassie blue staining of Input Recombinant MLKL.

(D) The dominant-negative effect of the phosphorylation site mutant MLKL on necrosis. RIP3-HeLa cells were transfected with WT or mutant MLKL. At 24 hr posttransfection, the cells were treated as indicated for another 24 hr. Cell viability was determined by measuring ATP levels. The data are presented as the mean ± SD of duplicate wells. The transfection efficiency was measured by western blot analysis.

(E) The effect of the phosphomimetic MLKL mutant on necrosis. Knockdown and rescue experiments in RIP3-HeLa cells were performed as in Figure 2C. Cell viability was determined by measuring ATP levels. The data are presented as the mean ± SD of duplicate wells.

(F) The MLKL levels in knockdown and rescue experiments were measured by western blot analysis.

See also Figure S5.

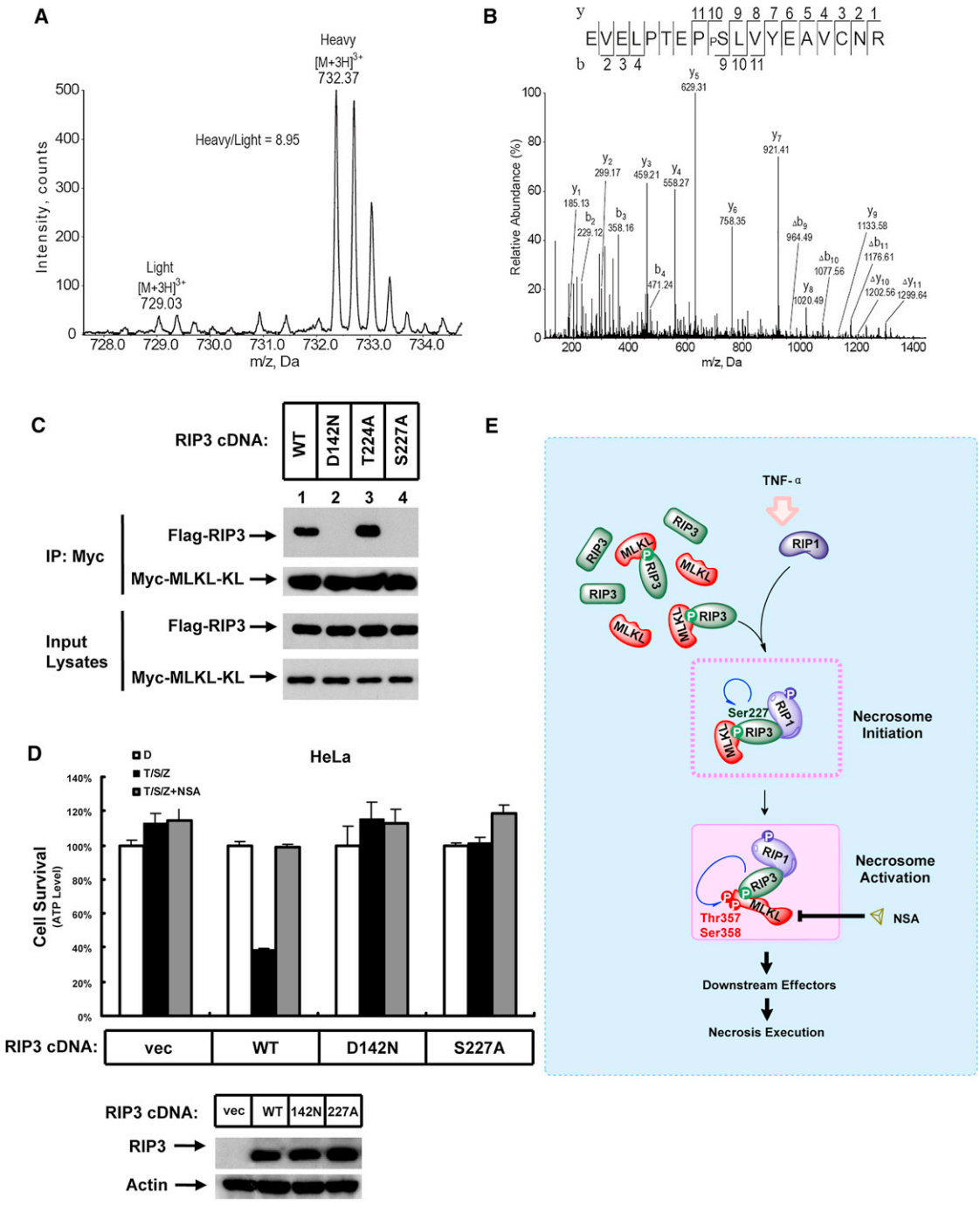

Figure 7. Identification and Characterization of Necrosis-Dependent Phosphorylation on RIP3

(A) Quantification of the RIP3-phosphorylated peptide. A SILAC experiment was performed as described in the Experimental Procedures, and a light and heavy isotope-labeled peptide pair was matched to a RIP3 single-phosphorylated peptide. The heavy/light peptide ratio was calculated as 8.95 based on the XIC of this peptide pair.

(B) Tandem mass (MS/MS) spectrum of the heavy isotope-labeled phosphorylated peptide as indicated in (A). The MS/MS spectrum identified this mono-phosphorylated peptide to be EVELPTEP$_p$SLVYEAVCNR, with S227 as the phosphorylated amino acid residue. The b and y type product ions are indicated in the spectrum. The cysteine residue in this peptide was carbamidomethylated. The symbol Δ refers to the neutral loss of a phosphoric acid.

(C) Pull-down analysis of MLKL with RIP3 phosphorylation site mutants. Flag-tagged WT or mutant RIP3 was cotransfected with Myc-tagged MLKL kinase-like domain in HeLa cells. Twenty-four hours posttransfection, whole-cell lysates were used for immunoprecipitation with an anti-Myc antibody, and the immunocomplexes were analyzed by western blot analysis using an anti-Flag antibody. Aliquots of 20 μg of whole-cell lysates were subjected to western blot analysis for Flag-RIP3 and Myc-MLKL levels (Input Lysates).

Necrosulfonamide, however, prevents necrosome from interacting with its downstream effectors.

Necrosulfonamide Inhibits MLKL-Mediated Necrosis by Blocking Its N-Terminal CC Domain Function

Necrosulfonamide efficiently blocks necrosis in human cells, but not mouse cells, which may explain why it was not detected by a similar screen using mouse L929 cells (Degterev et al., 2005). The reason for the species specificity of necrosulfonamide is that the cysteine at residue 86 in human MLKL that is covalently modified by necrosulfonamide is replaced by a tryptophan residue in mouse MLKL.

The site of MLKL at which the compound is bound indicates that the N-terminal CC domain of MLKL is important for MLKL's function. The binding of the compound to MLKL and RIP3-mediated phosphorylation of MLKL at its kinase-like domain seem to be independent events. The cysteine to alanine mutant at the amino acid residue 86 of MLKL retains the ability to transduce the necrosis signal, and the T357A/S358A double mutant can still bind necrosulfonamide, despite its inability to induce necrosis. Hence, it is likely that both the CC domain and the phosphorylated kinase-like region serve important functions in activating downstream necrosis effectors.

MLKL Connects the Necrosome with Its Downstream Effectors

Our results indicate that MLKL is a functional substrate for RIP3 kinase that serves as an adaptor protein for necrosis signal transduction. MLKL interacts with RIP3 through its kinase-like domain. In the absence of MLKL (or when its function is blocked by necrosulfonamide), RIP3 and RIP1 still bind to each other upon necrosis induction, resulting in a stable complex and higher levels of autophosphorylation. At this stage, RIP1 and RIP3 form discrete cytosolic punctae, but these punctae cannot expand without functional MLKL.

We believe that MLKL is critical for properly targeting the RIP3 necrosome to its functional downstream target(s), which most likely is located on cellular organelles such as mitochondria and/or lysosomes. Probing RIP3-interacting proteins in the presence and absence of necrosulfonamide may allow us to identify additional functional target(s) of RIP3. Indeed, we find that without MLKL, RIP3 fails to trigger phosphorylation on the mitochondrial protein phosphatase PGAM5S, which is an enzyme that is required for necrosis downstream of the RIP1/3 kinases (see the accompanying article by Wang et al., 2011 in this issue of *Cell*).

MLKL may also mediate signal transduction beyond RIP3 because it is more widely expressed than RIP3 in different cell types. It will therefore be interesting to identify the kinases with which MLKL interacts in the context of other signaling events. The compound necrosulfonamide may serve as a useful tool in dissecting these potential signaling pathways.

EXPERIMENTAL PROCEDURES

General Reagents and Methods

The following antibodies and reagents were used: anti-FLAG M2 monoclonal antibody and affinity gel (Sigma-Aldrich); anti-Myc affinity gel (Sigma-Aldrich); Flag-HRP, Myc-HRP, and V5-HRP (Sigma-Aldrich); biotin-HRP (Cell Signaling Technology); anti-MLKL polyclonal antibody (Sigma-Aldrich); anti-RIP1 monoclonal antibody (BD PharMingen); and anti-TNF-R1 (H-271) polyclonal antibody (Santa Cruz Biotechnology).

Cell Survival Assay

Cell survival assay was performed using the CellTiter-Glo Luminescent Cell Viability Assay kit. A CellTiter-Glo Assay (Promega) was performed according to the manufacturer's instructions. Luminescence was recorded with a Tecan GENios Pro plate reader.

Screen Assay Design

HT-29 cells were set up for screening the necrosis inhibitors. The detailed method is described in the Extended Experimental Procedures.

Cell Culture and Stable Cell Lines

RIP3-HeLa cells and RIP3-HT29 cells were established as described (He et al., 2009; Wang et al., 2011). Stable HeLa cell lines expressing the Tet repressor (HeLa-TetR cells) were selected with 10 μg/ml blasticidin after being transfected with pcDNA6/TR (Invitrogen). HeLa-TetR cells were transfected with a pcDNA3.1 plasmid encoding HA-3xFlag-RIP3 and were selected with 1 mg/ml G418 to establish the RIP3-HeLa cell line. The sources of other cell lines and the detailed culture conditions are described in the Extended Experimental Procedures.

Live-Cell Imaging and Immunofluorescence Staining

Live-cell imaging was obtained with a Nikon Ti inverted microscope and the PerkinElmer UltraVIEW VoX system. The detailed method of live-cell imaging and immunofluorescence staining are described in the Extended Experimental Procedures.

Immunoprecipitation and Immunoblotting

The cells were cultured on 10 cm dishes and grown to confluence. Cells at 90% confluence were washed once with PBS and harvested by scraping and centrifugation at 800 × *g* for 5 min. The harvested cells were washed with PBS and lysed for 30 min on ice in the lysis buffer. Cell lysates were then spun down at 12,000 × *g* for 20 min. The soluble fraction was collected, and the protein concentration was determined by Bradford assay. Next, 1 mg of extracted protein in lysis buffer was immunoprecipitated overnight with anti-Flag or anti-Myc affinity gel (Sigma-Aldrich) at 4°C. The immunoprecipitates were washed three times with lysis buffer. The beads were then eluted with 0.5 mg/ml of the corresponding antigenic peptide for 4 hr or directly boiled in 1% SDS loading buffer.

Gene Knockdown and Rescue

On day 1, RIP3-HeLa cells were plated in 96-well assay plates and treated with doxycycline. On day 2, each well was transfected with 2.5 pmol of siRNA against specific genes or luc as negative control along with 0.05 μg of a cDNA bearing silent mutations in the siRNA-targeted region or vector plasmid as a mock transfection control. On day 3, the cells were treated with indicated stimuli for 24 hr. Cell viability was determined by measuring ATP levels.

(D) The effect of RIP3-S227 phosphorylation on necrosis. The WT and kinase-dead mutant (D142N) and phosphorylation site mutant (S227A) were used to transfect HeLa cells. The cells were then treated with indicated necrosis-inducing agents. Cell viability was determined by measuring ATP levels. The data are presented as the mean ± SD of duplicate wells. The levels of WT and mutant RIP3 were measured by western blot analysis (C).
(E) Model of functional necrosome formation. See Discussion for details.
See also Figure S7.

Biotin-NSA Synthesis

The biotin-NSA was synthesized as described in the Extended Experimental Procedures.

Biotin-NSA Precipitation

The cells were plated on 10 cm dishes and grown to confluence for 1 day. On day 2 the cells were transfected with the indicated siRNA or cDNA. The cells were harvested and lysed in lysis buffer as described above 24 or 48 hr after transfection with cDNA or siRNA, respectively. Biotin-NSA (20 nmol) was pre-incubated with 20 μl streptavidin agarose (Invitrogen) for 2 hr at 4°C. The beads were then washed two times in lysis buffer. The necrosulfonamide-bound agarose was then incubated with cell lysates overnight at 4°C. Nonbiotin-NSA (or its derivatives) was included in the lysates as a binding competitor. The following day, the beads were washed four times with lysis buffer, then directly boiled in 1% SDS loading buffer.

In Vitro Kinase Assay

RIP1 and RIP3 were immunoprecipitated with an anti-Flag antibody. The Flag beads were washed three times with kinase buffer (50 mM HEPES [pH 7.5], 10 mM $MgCl_2$, 50 mM NaCl, 0.02% BSA, 150 μM ATP, and 1 mM DTT), then incubated with 2 μCi of [^{32}P]γ-ATP at 37°C for 1 hr with the artificial substrate MBP or purified recombinant MLKL. The reaction mixtures were then subjected to SDS-PAGE followed by autoradiography.

Preparation of Recombinant MLKL

The human MLKL recombinant protein was generated using Bac-to-Bac Baculovirus Expression Systems (Invitrogen; catalog # 10359-016). The details of preparation of recombinant MLKL are described in the Extended Experimental Procedures.

SUPPLEMENTAL INFORMATION

Supplemental Information includes Extended Experimental Procedures and seven figures and can be found with this article online at doi:10.1016/j.cell.2011.11.031.

ACKNOWLEDGMENTS

We would like to express our gratitude to the High-throughput Screening Facility at the University of Texas Southwestern Medical Center for help with the chemical screening. We thank Dr. Agata Rybarska for critically reading the manuscript. This work was supported by the Howard Hughes Medical Institute and a grant from the National Cancer Institute (NCI) (PO1 CA 95471). The work in Beijing was supported by National High Technology Projects 863 (2008AA022318 [to X.W.] and 2008AA022317 [to X.L.]) and 973 (2010CB835400) from Chinese Ministry of Science and Technology.

Received: June 22, 2011
Revised: October 25, 2011
Accepted: November 10, 2011
Published: January 19, 2012

REFERENCES

Ashkenazi, A., and Dixit, V.M. (1999). Apoptosis control by death and decoy receptors. Curr. Opin. Cell Biol. *11*, 255–260.

Cauwels, A., Janssen, B., Waeytens, A., Cuvelier, C., and Brouckaert, P. (2003). Caspase inhibition causes hyperacute tumor necrosis factor-induced shock via oxidative stress and phospholipase A2. Nat. Immunol. *4*, 387–393.

Cho, Y.S., Challa, S., Moquin, D., Genga, R., Ray, T.D., Guildford, M., and Chan, F.K. (2009). Phosphorylation-driven assembly of the RIP1-RIP3 complex regulates programmed necrosis and virus-induced inflammation. Cell *137*, 1112–1123.

Declercq, W., Vanden Berghe, T., and Vandenabeele, P. (2009). RIP kinases at the crossroads of cell death and survival. Cell *138*, 229–232.

Degterev, A., Huang, Z., Boyce, M., Li, Y., Jagtap, P., Mizushima, N., Cuny, G.D., Mitchison, T.J., Moskowitz, M.A., and Yuan, J. (2005). Chemical inhibitor of nonapoptotic cell death with therapeutic potential for ischemic brain injury. Nat. Chem. Biol. *1*, 112–119.

Degterev, A., Hitomi, J., Germscheid, M., Ch'en, I.L., Korkina, O., Teng, X., Abbott, D., Cuny, G.D., Yuan, C., Wagner, G., et al. (2008). Identification of RIP1 kinase as a specific cellular target of necrostatins. Nat. Chem. Biol. *4*, 313–321.

Du, C., Fang, M., Li, Y., Li, L., and Wang, X. (2000). Smac, a mitochondrial protein that promotes cytochrome c-dependent caspase activation by eliminating IAP inhibition. Cell *102*, 33–42.

Ellis, R.E., Yuan, J.Y., and Horvitz, H.R. (1991). Mechanisms and functions of cell death. Annu. Rev. Cell Biol. *7*, 663–698.

Feng, S., Yang, Y., Mei, Y., Ma, L., Zhu, D.E., Hoti, N., Castanares, M., and Wu, M. (2007). Cleavage of RIP3 inactivates its caspase-independent apoptosis pathway by removal of kinase domain. Cell. Signal. *19*, 2056–2067.

Gallo, K.A., and Johnson, G.L. (2002). Mixed-lineage kinase control of JNK and p38 MAPK pathways. Nat. Rev. Mol. Cell Biol. *3*, 663–672.

He, S., Wang, L., Miao, L., Wang, T., Du, F., Zhao, L., and Wang, X. (2009). Receptor interacting protein kinase-3 determines cellular necrotic response to TNF-alpha. Cell *137*, 1100–1111.

Kaiser, W.J., Upton, J.W., Long, A.B., Livingston-Rosanoff, D., Daley-Bauer, L.P., Hakem, R., Caspary, T., and Mocarski, E.S. (2011). RIP3 mediates the embryonic lethality of caspase-8-deficient mice. Nature *471*, 368–372.

Kerr, J.F., Wyllie, A.H., and Currie, A.R. (1972). Apoptosis: a basic biological phenomenon with wide-ranging implications in tissue kinetics. Br. J. Cancer *26*, 239–257.

Kroemer, G., and Martin, S.J. (2005). Caspase-independent cell death. Nat. Med. *11*, 725–730.

Li, L., Thomas, R.M., Suzuki, H., De Brabander, J.K., Wang, X., and Harran, P.G. (2004). A small molecule Smac mimic potentiates TRAIL- and TNFalpha-mediated cell death. Science *305*, 1471–1474.

Li, P., Nijhawan, D., Budihardjo, I., Srinivasula, S.M., Ahmad, M., Alnemri, E.S., and Wang, X. (1997). Cytochrome c and dATP-dependent formation of Apaf-1/caspase-9 complex initiates an apoptotic protease cascade. Cell *91*, 479–489.

Lin, Y., Devin, A., Rodriguez, Y., and Liu, Z.G. (1999). Cleavage of the death domain kinase RIP by caspase-8 prompts TNF-induced apoptosis. Genes Dev. *13*, 2514–2526.

Oberst, A., Dillon, C.P., Weinlich, R., McCormick, L.L., Fitzgerald, P., Pop, C., Hakem, R., Salvesen, G.S., and Green, D.R. (2011). Catalytic activity of the caspase-8-FLIP(L) complex inhibits RIPK3-dependent necrosis. Nature *471*, 363–367.

Sato, S., Kwon, Y., Kamisuki, S., Srivastava, N., Mao, Q., Kawazoe, Y., and Uesugi, M. (2007). Polyproline-rod approach to isolating protein targets of bioactive small molecules: isolation of a new target of indomethacin. J. Am. Chem. Soc. *129*, 873–880.

Scaffidi, C., Fulda, S., Srinivasan, A., Friesen, C., Li, F., Tomaselli, K.J., Debatin, K.M., Krammer, P.H., and Peter, M.E. (1998). Two CD95 (APO-1/Fas) signaling pathways. EMBO J. *17*, 1675–1687.

Thornberry, N.A., and Lazebnik, Y. (1998). Caspases: enemies within. Science *281*, 1312–1316.

Trichonas, G., Murakami, Y., Thanos, A., Morizane, Y., Kayama, M., Debouck, C.M., Hisatomi, T., Miller, J.W., and Vavvas, D.G. (2010). Receptor interacting protein kinases mediate retinal detachment-induced photoreceptor necrosis and compensate for inhibition of apoptosis. Proc. Natl. Acad. Sci. USA *107*, 21695–21700.

Upton, J.W., Kaiser, W.J., and Mocarski, E.S. (2010). Virus inhibition of RIP3-dependent necrosis. Cell Host Microbe *7*, 302–313.

Vercammen, D., Beyaert, R., Denecker, G., Goossens, V., Van Loo, G., Declercq, W., Grooten, J., Fiers, W., and Vandenabeele, P. (1998). Inhibition

of caspases increases the sensitivity of L929 cells to necrosis mediated by tumor necrosis factor. J. Exp. Med. *187*, 1477–1485.

Verhagen, A.M., Ekert, P.G., Pakusch, M., Silke, J., Connolly, L.M., Reid, G.E., Moritz, R.L., Simpson, R.J., and Vaux, D.L. (2000). Identification of DIABLO, a mammalian protein that promotes apoptosis by binding to and antagonizing IAP proteins. Cell *102*, 43–53.

Wang, C., and Youle, R.J. (2009). The role of mitochondria in apoptosis. Annu. Rev. Genet. *43*, 95–118.

Wang, Z., Jiang, H., Chen, S., Du, F., and Wang, X. (2011). The mitochondrial phosphatase PGAM5 functions at the convergent point of multiple necrotic death pathways. Cell *148*, this issue, 228–243.

Yang, Q.H., and Du, C. (2004). Smac/DIABLO selectively reduces the levels of c-IAP1 and c-IAP2 but not that of XIAP and livin in HeLa cells. J. Biol. Chem. *279*, 16963–16970.

Zhang, D.W., Shao, J., Lin, J., Zhang, N., Lu, B.J., Lin, S.C., Dong, M.Q., and Han, J. (2009). RIP3, an energy metabolism regulator that switches TNF-induced cell death from apoptosis to necrosis. Science *325*, 332–336.

EXTENDED EXPERIMENTAL PROCEDURES

Plasmids and Antibodies

Human and mouse MLKL cDNA were purchased from Open Biosystems. Full-length human MLKL and RIP3 were subcloned into the pTK-GLuc vector (NEB) under the control of the thymidine kinase (TK) promoter or into pcDNA3.1 (Invitrogen) under the control of the cytomegalovirus (CMV) promoter. Deletion mutants were generated using standard PCR methods, and point mutations were generated using the Quikchange Site-Directed Mutagenesis Kit (Stratagene) according to the manufacturer's instructions.

The following antibodies and reagents were used: anti-FLAG M2 monoclonal antibody and affinity gel (Sigma); anti-Myc affinity gel (Sigma); Flag-HRP and Myc-HRP (Sigma); biotin-HRP (Cell Signaling Tech); anti-MLKL polyclonal antibody (Sigma); anti-RIP1 monoclonal antibody (BD PharMingen); anti-TNF-R1 (H-271) polyclonal antibody (Santa Cruz Biotech).

Screen Assay Design

On day one, 2,000 HT-29 cells were split into each well of a 384-well assay plate. On day two, necrosis was induced by adding final concentrations of 20 ng/ml TNF-α (T), 100 nM Smac mimetic (S), and 20 μM z-VAD (Z) to the well. Identical concentrations of these necrosis-inducing agents were used in subsequent experiments unless otherwise stated. Concurrently, individual compounds from a chemical library of ~200,000 compounds were delivered into each well at a final concentration of 10 μM. Cell viability in this and subsequent panels was determined by measuring ATP levels by Cell Titer-Glo assay after 24 hrs.

RNA Interference

Human and mouse siRNA oligos were obtained from Dharmacon's ON-TARGET plus siRNA pool of 4 oligos. The following sequence was used in the knockdown and rescue experiments: human MLKL (5′-CAAACUUCCUGGUAACUCA-3′;). Human RIP1 (5′;-CCACUAGUCUGACGGAUAA-3′;), RIP3 (5′;-CCAGAGACCUCAACUUUCA-3′;) and luciferase (5′;-CGUACGCGGAAUACUUCGA-3′;) oligos were synthesized by Dharmacon. The cells were transfected with the siRNA oligos using Lipofectamine2000 (Invitrogen) according to the manufacturer's instructions.

Cell Culture and Stable Cell Lines

HT-29 cells were cultured in McCoy's 5A culture medium (Invitrogen). HeLa, Panc-1, NIH/3T3 and L929 cells were cultured in Dulbecco's modified Eagle's medium (Invitrogen). FADD-null Jurkat cells and MKN-45 cells were grown in RPMI-1640 medium (Hyclone). All media were supplemented with 10% FBS (Invitrogen) and 100 units/ml penicillin/streptomycin (Hyclone). The cells were transfected using Lipofectamine2000 (Invitrogen) according to the manufacturer's instructions. Stable HeLa cell lines expressing the Tet repressor (HeLa-TetR cells) were selected with 10 μg/ml blasticidin after being transfected with pcDNA6/TR (Invitrogen). HeLa-TetR cells were transfected with a pcDNA3.1 plasmid encoding HA-3xFlag-RIP3 and were selected with 1 mg/ml G418 to establish the RIP3-HeLa cell line.

Cell Survival Assay

Cell survival assay was performed using the Cell Titer-Glo Luminescent Cell Viability Assay kit. A CellTiter-Glo assay (Promega) was performed according to the manufacturer's instructions. Luminescence was recorded with a Tecan GENios Pro plate reader.

Live-Cell Imaging

On day one, HeLa cells were cultured in 35-mm glass-bottom culture dishes (MatTek) and transfected with 0.8 μg of human RIP3 cDNA with an N-terminal mCherry-tag the next day. On day three, the cells were plated in a 37°C imaging station chamber and treated with TNF-α/Smac mimetic/z-VAD. Images were obtained with a Nikon Ti inverted microscope and the PerkinElmer UltraVIEW VoX system. Time-lapse images were captured at 5-min intervals using a Nikon PLAN APO 60× oil objective. The images were processed using Volocity software.

Immunofluorescence Staining

HeLa cells were cultured in a chamber slide (Nunc Lab-Tek Chamber Slide system) as previously described (Du et al., 2000). The cell treatment was terminated by washing with PBS followed by fixation in freshly prepared 4% paraformaldehyde in PBS for 10 min. The fixed cells were washed three times with PBS and then permeabilized in 0.25% Triton X-100 in PBS for 10 min. The cells were then blocked for 30 min in blocking buffer (0.25% Triton X-100 and 5% BSA in PBS). The primary antibodies were diluted in blocking buffer, and the cells were immunolabeled at 4°C overnight. The cells were washed three times with PBS followed by a one-hour incubation with a fluorescein-conjugated secondary antibody (Invitrogen). DAPI was used to stain the nuclei. Duplicate cultures were examined, and similar results were obtained in at least three independent experiments.

Gene Knockdown and Rescue

On day one, RIP3-HeLa cells were plated in 96-well assay plates and treated with doxycycline. On day two, each well was transfected with 2.5 pmol of siRNA against specific genes or luciferase (luc) as negative control along with 0.05 μg of a cDNA bearing silent

mutations in the siRNA-targeted region or vector plasmid as a mock transfection control. On day three, the cells were treated with indicated stimuli for 24 hrs. Cell viability was determined by measuring ATP levels.

Preparation of the P15 Fraction from RIP3-HeLa Cells

Harvested cell pellets were resuspended in a 5× volume of buffer A (20 mM HEPES, pH 7.4, 40 mM KCl, 1.5 mM $MgCl_2$, 1 mM EDTA, 1 mM EGTA, 0.1 mM PMSF and 250 mM sucrose) and incubated on ice for 30 min. The cells were lysed by passing through a 22-G needle or glass Dounce homogenizer 24 times. After centrifugation at 1,000×*g* for 10 min, the supernatant was harvested and re-centrifuged at 15,000×*g* for 10 min. The supernatant was saved as the S15 fraction. The pellet was re-suspended in a 5x volume of lysis buffer (20 mM HEPES, pH 7.4, 150 mM NaCl, 1% Triton X-100, 10% glycerol, and complete protease inhibitor [Roche]) and incubated on ice for 30 min. After centrifugation at 15,000×*g* for 10 min, the supernatant was harvested as the P15 fraction.

Immunoprecipitation and Immunoblotting

Unless otherwise noted, HeLa cells were used for the transfections and analyses of protein-protein interactions. The cells were cultured on 10-cm dishes and grown to confluence. Cells at 90% confluence were washed once with phosphate-buffered saline (PBS) and harvested by scraping and centrifugation at 800×*g* for 5 min. The harvested cells were washed with PBS and lysed for 30 minutes on ice in the lysis buffer. Cell lysates were then spun down at 12,000×*g* for 20 min. The soluble fraction was collected, and the protein concentration was determined by Bradford assay. Next, 1 mg of extracted protein in lysis buffer was immunoprecipitated overnight with anti-Flag or anti-Myc affinity gel (Sigma) at 4°C. The immunoprecipitates were washed three times with lysis buffer. The beads were then eluted with 0.5 mg/ml of the corresponding antigenic peptide for 4 hours or directly boiled in 1×SDS loading buffer.

Biotinylated Necrosulfonamide Precipitation

The cells were plated on 10-cm dishes and grown to confluence for one day. On day two, the cells were transfected with the indicated siRNA or cDNA. The cells were harvested and lysed in lysis buffer as described above 24 or 48 hours after transfection with cDNA or siRNA, respectively. Biotinylated necrosulfonamide (20 nmol) was preincubated with 20 μl streptavidin agarose (Invitrogen) for 2 hrs at 4°C. The beads were then washed two times in lysis buffer. The necrosulfonamide-bound agarose were then incubated with cell lysates overnight at 4°C. Non-biotinylated necrosulfonamide (or its derivatives) was included in the lysates as a binding competitor. The following day, the beads were washed four times with lysis buffer, then directly boiled in 1×SDS loading buffer.

In Vitro Kinase Assay

RIP1 and RIP3 were immunoprecipitated with an anti-Flag antibody. The Flag beads were washed three times with kinase buffer (50 mM HEPES, pH 7.5, 10 mM $MgCl_2$, 50 mM NaCl, 0.02% BSA, 150 μM ATP and 1 mM DTT), then incubated with 2 μCi of [32P]γ-ATP at 37°C for 1 hour with the artificial substrate MBP or purified recombinant MLKL. The reaction mixtures were then subjected to SDS-PAGE followed by autoradiography.

Production of Recombinant MLKL Protein in a Baculovirus Expression System

The cDNAs encoding wild type MLKL or mutant MLKL fused with a GST-tag at the N-terminal were subcloned into the baculovirus expression vector pFastBacI (Life Technologies, Inc.). The expression plasmid was transformed into DH10Bac *E. coli* cells (Life Technologies, Inc.). The recombinant viral DNA bacmid was purified according to the Bac-To-Bac Baculovirus Expression procedure and confirmed by PCR amplification analysis. Recombinant MLKL was generated as described previously (Zou et al., 1999). GST was cleaved from recombinant MLKL using precision protease (GE Healthcare).

Mass Spectrometric Analysis

Protein bands were excised from the SDS-PAGE gel, de-stained and then reduced in 10 mM DTT at 56°C for 30 min, followed by alkylation in 55 mM iodoacetamide for 1 hr in the dark. The protein bands were then digested in-gel with sequencing-grade trypsin (10 ng/μl trypsin, 50 mM ammonium bicarbonate, pH 8.0) overnight at 37°C. The peptides were extracted with 5% formic acid/50% acetonitrile followed by 0.1% formic acid/75% acetonitrile and then concentrated to a volume of ~20 μl. The extracted peptides were separated in an analytical capillary column (50 μm × 10 cm) that was packed with 5-μm spherical C18 reverse phase material (YMC, Kyoto, Japan). An Agilent 1100 binary pump was used to generate the HPLC gradient as follows: 0-5% B for 5 min, 5-40% B for 25 min, 40-100% B for 15 min (A = 0.1 M acetic acid in water; B = 0.1 M acetic acid/70% acetonitrile). The eluted peptides were sprayed into a QSTAR XL mass spectrometer (AB Sciex, Foster City, CA, USA) that was equipped with a nano-ESI ion source. The mass spectrometer was operated in information-dependent mode with one MS scan followed by three MS/MS scans for each cycle. Database searches were performed on an in-house Mascot server (Matrix Science Ltd., London, UK), and the following variable modifications were included: methionine oxidation, cysteine carbamidomethylation, and serine, threonine, and tyrosine phosphorylation.

For SILAC quantification, the Mascot search results were imported to the open-source software MSQuant (http://msquant.sourceforge.net) to calculate the ratios of the heavy/light peptide pairs according to their extracted ion chromatograms (XICs). The quantification results from all peptide pairs were manually checked to ensure their accuracy.

Biotinylated Necrosulfonamide Synthesis

Biotin-LC-proline acid (14 mg, 0.01 mmol) and primary amine (16 mg, 0.03 mmol) were dissolved in 1 ml of DMF at room temperature under the argon atmosphere, DIEA (17μL, 0.1 mmol) was added, and followed by HATU (12 mg, 0.03 mmol). The resulting solution was stirred at room temperature for 18 hours. The solvent was removed under high vacuum and the residue was purified by the reversed-phase HPLC[Waters Auto Purification LC/MS system (3100 Mass Detector, 2545 Binary Gradient Module, 2767 Sample Manager, and 2998 Photodiode Array Detector), X-Bridge C18 column (19x150mm), CH3CN/H2O(with 0.5%TFA) gradient 10/90∼30/70 (0-3 min), 30/70∼45/55(12-15 min), 45/55∼100:0 (15-20 min), 17 ml/min] to afford the desired probe as a colorless oil (6 mg, 32%).HRMS (ESI) [M + H+] calculated for C87H119N20O20S3: 1859.80661, found: 1859.80879.

SUPPLEMENTAL REFERENCE

Zou, H., Li, Y., Liu, X., and Wang, X. (1999). An APAF-1 cytochrome c multimeric complex is a functional apoptosome that activates procaspase-9. J. Biol. Chem. *274*, 11549–11556.

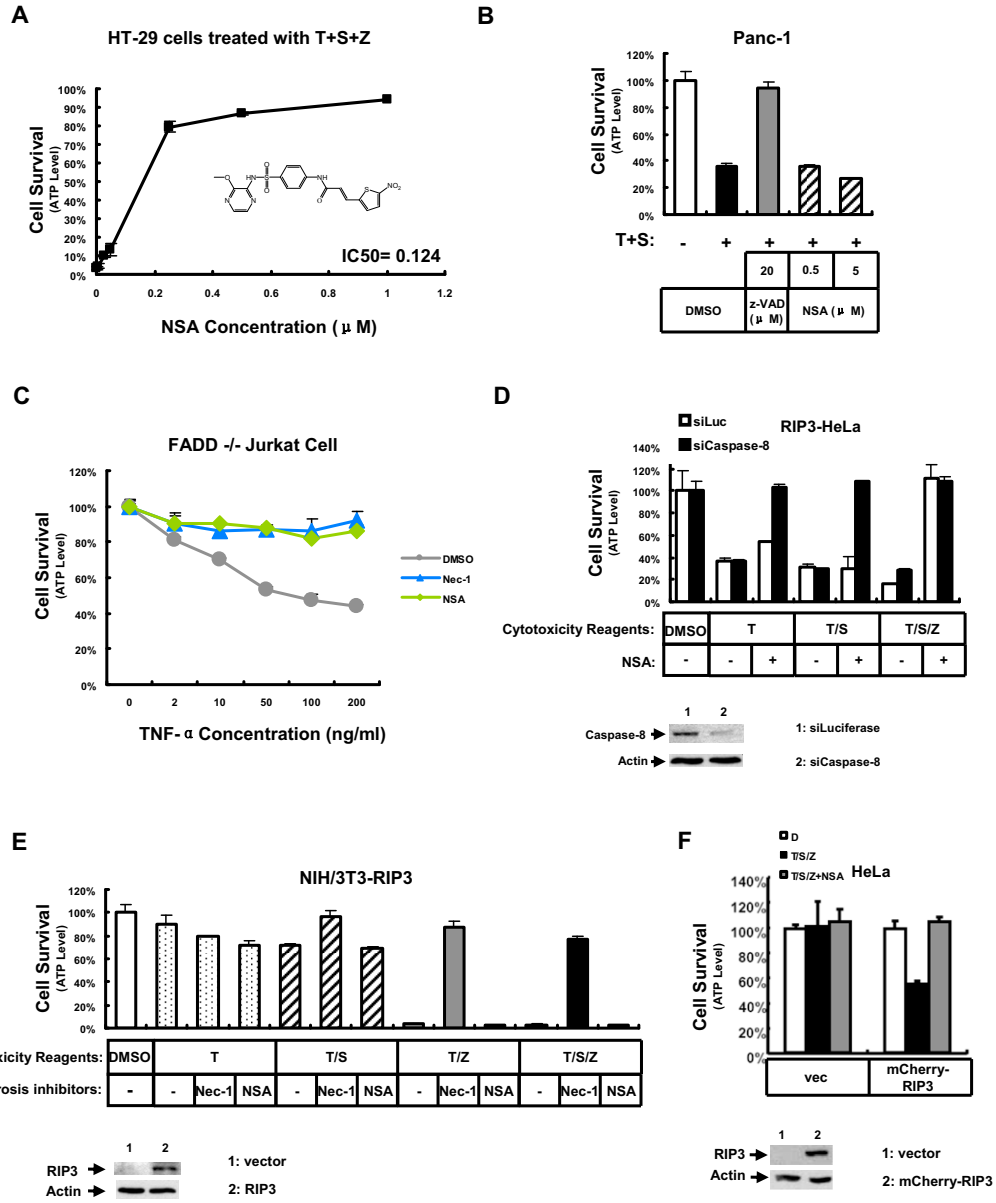

Figure S1. Necrosulfonamide Specifically Inhibits Necrosis in Multiple Human Cell Lines, Related to Figure 1

(A) Dose-response curve (in μM) of Necrosulfonamide (NSA) in HT-29 cells treated with TNF-α/smac mimetic/z-VAD for 24 hrs. Single replicate 7-point dose-response was done. Cell viability was determined by measuring ATP levels after 24 hrs. Data are represented as mean ± standard deviation of duplicates.

(B) Pancreatic cancer Panc-1 cells were treated as indicated for 24 hrs. Cell viability was determined by measuring ATP levels. The data are represented as the mean ± standard deviation of duplicates.

(C) NSA and Nec-1 inhibits TNF-α alone induced necrosis on FADD-null Jurkat cells. The cells were treated with TNF-α at indicated concentrations. Cell death was blocked by adding NSA (0.5 μM) or Nec-1 (10 μM). Cell viability was determined by measuring ATP levels. The data are represented as the mean ± standard deviation of duplicates.

(D) Necrosis induced by TNF-α after knockdown of caspase-8. Knockdown of Caspase-8 in RIP3-HeLa cells was described in Experimental Procedures. The cells were then treated with the indicated stimuli. The data are presented as the mean ± standard deviation of duplicate wells. The knockdown and rescue efficiencies were measured by western blot analysis in the lower panel.

(E) TNF-α/ z-VAD-fmk versus TNF-α/Smac mimetic/z-VAD-fmk induced necrosis in NIH/3T3 cells. NIH/3T3 cells were plated in 96-well assay plates and transfected with 0.1 μg of plasmid containing cDNA encoding mouse RIP3. At 24 hrs posttransfection, the cells were treated with indicated stimuli for 24 hrs. Cell viability was determined by measuring ATP levels. The data are presented as the mean ± standard deviation of duplicate wells. The transfection efficiency was quantified by western blot analysis.

(F) Wild type HeLa cells were transfected with 0.02 μg of cDNA encoding human RIP3 with an N-terminal mCherry tag. At 24 hrs posttransfection, cells were treated as indicated. Cell viability was determined by measuring ATP levels after 24 hrs. Data are represented as mean ± standard deviation of duplicates. Transfection efficiency was assessed by western blot.

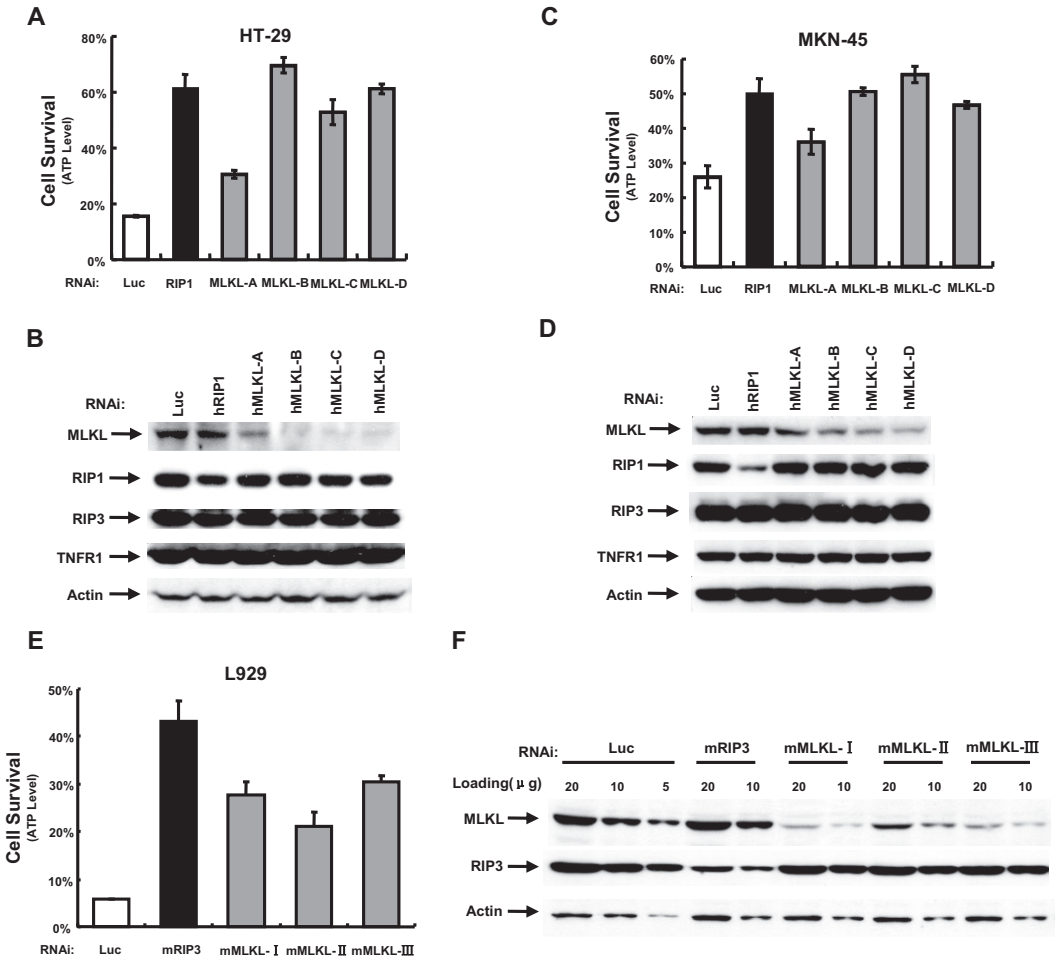

Figure S2. Knockdown of MLKL Inhibits Necrosis in Both Human and Mouse Cell Lines, Related to Figure 2

Human colon cancer HT-29 cells, human gastric cancer MKN-45 cells and mouse fibrosarcoma L929 cells were set up for necrotic cell death experiment. Cells were transfected with multiple small interfering RNAs (siRNAs) against MLKL. At 48 hrs posttransfection, cells were treated as indicated for 24 hrs. Cell viability was determined by measuring ATP levels (A, C, and E). Data are represented as mean ± standard deviation of duplicates. The knockdown efficiency was measured by western blots in the lower panel (B, D, and F). To avoid off-targeting effect, the other major components of necrosis pathway have been detected using western blot.

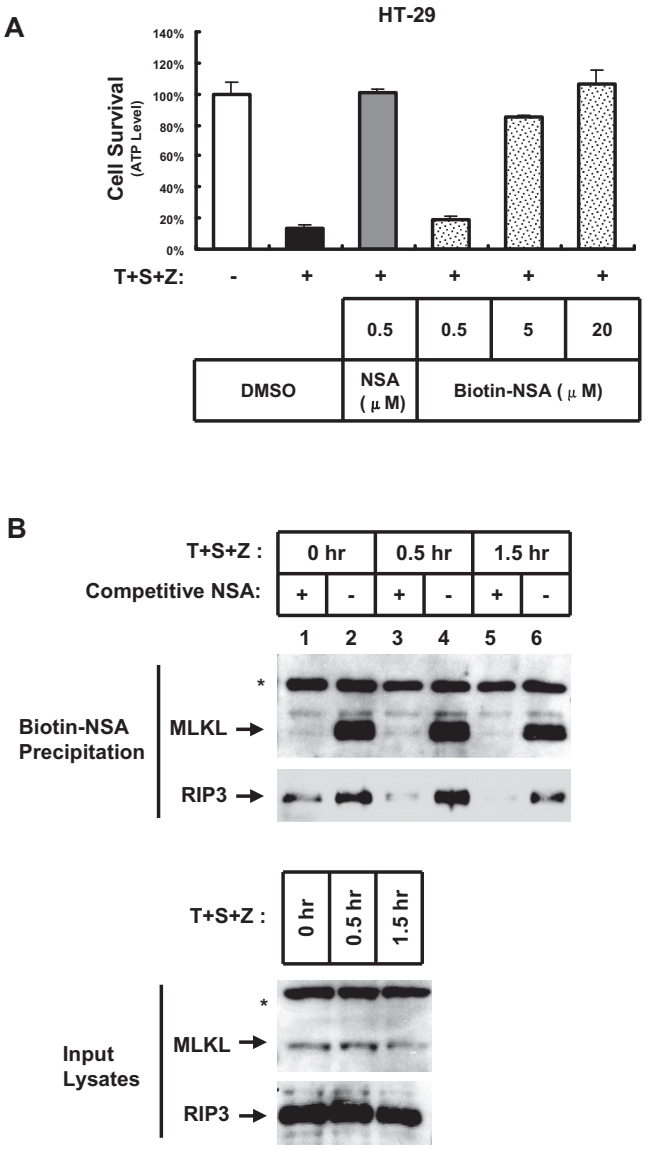

Figure S3. Biotinylated Necrosulfonamide Interacts with Endogenous MLKL, Related to Figure 3

(A) Dose-dependent inhibition of necrosis by biotinylate necrosulfonamide (bio-NSA).

(B) HT-29 cells were stimulated with TNF-α/Smac mimetic/z-VAD-fmk for the indicated time. Aliquots (1 mg) of whole-cell lysate from the cells were overnight incubated with biotinylated necrosulfonamide (biotin-NSA) at 4°C. The biotinylated compound was collected using streptavidin-conjugated beads, and the proteins that were bound to the beads were analyzed by SDS-PAGE followed by western blotting using antibodies against either MLKL or RIP3. Where indicated, non-biotinylated necrosulfonamide (NSA) was added to the lysates as competitive baits. Aliquots of 20 μg of whole-cell lysates were subjected to western blot analysis to measure the input RIP3 and MLKL levels. The asterisk (*) denotes a cross-reacting band.

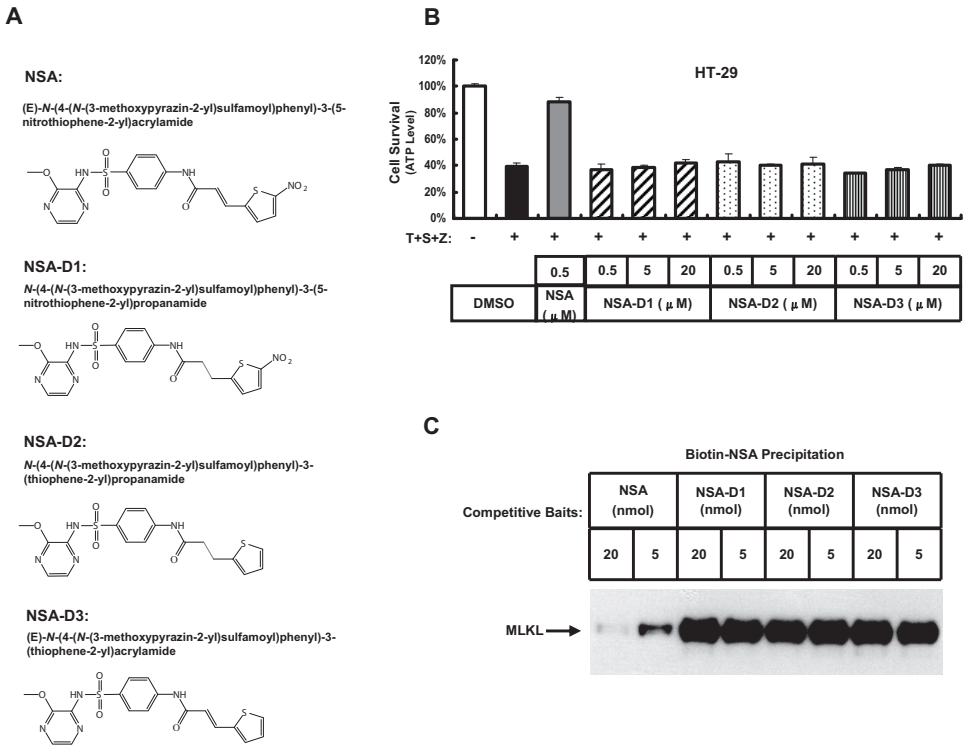

Figure S4. Characterization the Functional Groups of Necrosulfonamide, Related to Figure 4

(A) Chemical structure of necrosulfonamide (NSA) and the derivative compounds (NSA-D1, NSA-D2, NSA-D3). The structures of the alterative functional groups are labeled in red.

(B) HT-29 cells were set up for necrotic cell death analysis. Cells were treated as indicated for 24 hrs. Cell viability was determined by measuring ATP levels after 24 hrs. Data are represented as mean ± standard deviation of duplicates.

(C) Precipitation analysis of necrosulfonamide versus the derivatives with MLKL. At 24 hrs posttransfection of Myc-tagged cDNA of MLKL in RIP-HeLa cells, 1 mg aliquots of whole-cell lysates from HeLa cells were used for one condition of precipitation analysis with biotinylated necrosulfonamide. As indicated, the non-biotinylated necrosulfonamide or the derivatives was included in the lysates as competitive baits. The pellets of necrosulfonamide conjugates were analyzed by western blotting using anti-Myc antibody.

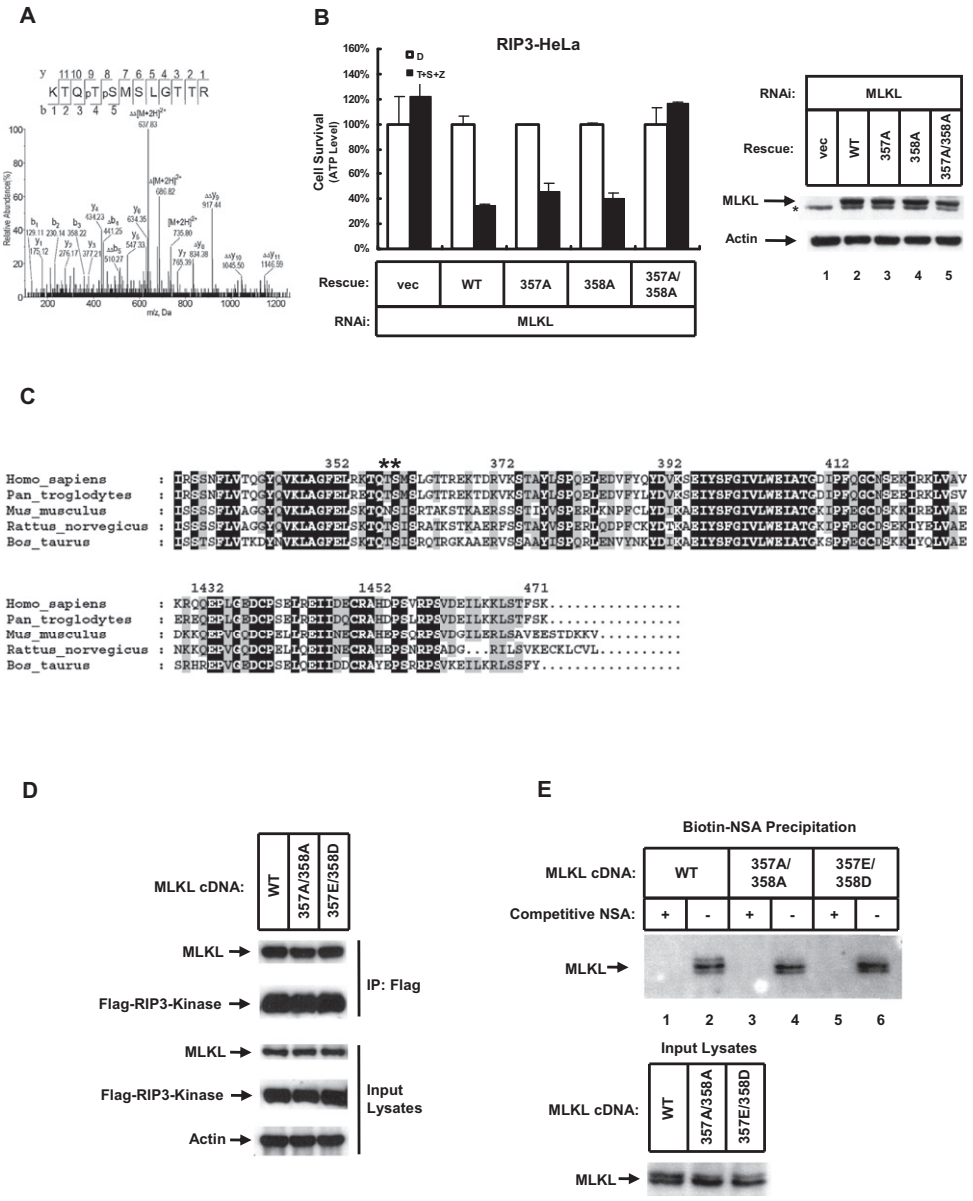

Figure S5. Characterization of the Phosphorylation Sites on MLKL, Related to Figure 6

(A) Mass spectra of the MLKL phosphorylated peptide KTQPTPSMSLGTTR. Tandem mass (MS/MS) spectrum of the heavy isotope labeled phosphorylated peptide. The b- and y- type product ions are indicated. The symbol refers to neutral loss of a phosphoric acid.

(B) Effect of single phospho-site mutation on the rescue phenotype of MLKL knockdown cells. RIP3-HeLa cells were co-transfected with siRNAs against MLKL and the cDNA encoding the indicated siRNA-resistant wild type or mutant MLKL. Knockdown and rescue experiments on RIP3-HeLa cells were performed as described in Experimental Procedures. At 48 hrs post transfection, cells were treated with indicated stimuli for 24 hrs. Cell viability was determined by measuring ATP levels. Data are represented as mean ± standard deviation of duplicates. The knockdown and rescue efficiency were measured by western blots as shown in the right panel.

(C) Alignment of amino acid sequences of MLKL orthologs in five vertebrate species. Identical amino acid residues in the sequences are shaded in black. Amino acid residues conserved in 80% or more of the sequences are shaded in grey. The putative phosphorylation residues are denoted by asterisks (*).

(D) The effect of phosphorylation site mutation on MLKL-RIP3 interaction. HeLa cells were co-transfected with Flag-tagged RIP3 kinase domain and Myc-tagged phosphorylation site mutant MLKL. At 24 hrs posttransfection, immunoprecipitation with anti-Flag antibody was performed as described in Experimental Procedures. RIP3 kinase domain conjugates (Flag IP) were analyzed by western blots using anti-Myc antibody. Representation of the examined proteins in the input lysates is shown in the bottom panel.

(E) Biotinylated necrosulfonamide pull-down analysis of wild type MLKL and phosphorylation-site mutant MLKL. Aliquots (1 mg) of whole-cell lysates from HeLa cells transfected with Myc-tagged MLKL were used for biotinylated necrosulfonamide pull-down analysis as described in Experimental Procedures. Aliquots of 20 μg whole cell lysates were subjected to SDS-PAGE analysis of wild type MLKL and phosphorylation site mutant MLKL levels. Representation of the examined proteins in the input lysates is shown (Input Lysates).

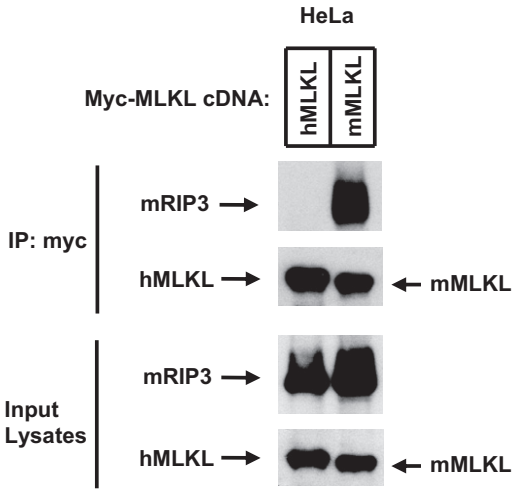

Figure S6. Species-Specific Binding between MLKL and RIP3, Related to Figure 5

Myc-tagged human or mouse MLKL was co-transfected with Flag-tagged mouse RIP3 in HeLa cells. Twenty-four hours posttransfection, whole-cell lysates were used for immunoprecipitation with anti-Myc (MLKL) antibody and the immune-complexes were analyzed by western blotting using anti-Myc and anti-Flag antibodies. Representation of the examined proteins in the input lysates is shown (Input Lysates).

A

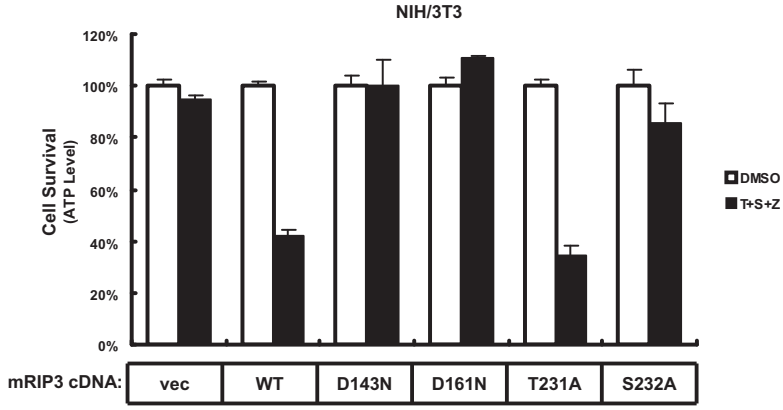

B

```
                                198                 218       *       238                 258
Homo_sapiens       : EPGGTLGYLAPELFVNVNRKASTASDVYSFGILMWAVFAGREVELPTEPSLVYEAVCNRQNRPSLAELPQAGPETPGLEGLKELMQLCWSSEPKD
Pan_troglodytes    : EPGGTLGYLAPELFVNVNRKASTASDVYSFGILMWAVFAGREVELPTEPSLVYEAVGNRQNRPSLAELPQAGPETPGLEGLKELMQLCWSSKPKD
Mus_musculus       : DSGGTLAYLDPELLFDVNLKASKASDVYSFGILVWAVFAGREAELVDKTSLIRETVCDRQSRPPLTELPPGSPETPGLEKLKELMIHCWGSQSEN
Rattus_norvegicus  : DSGGTLAYLAPELL.DNDGKASKASDVYSFGVLVWTVFAGREAEVVDKTSLIRGAVCNRQRRPPLTELPPDSPETPGLEGLKELMTHCWSSEPKD
Canis_familiaris   : ...SAPAYLAPELLPDVNRKASMASDVYSFGILMWAVFAGREAEIVAQTSPVREAVCERQIRPPLTKLPLPSPETPGLERLKALMQHCWSHEPKD
Bos_taurus         : ESGCTPAYLAPELLANINQKASRASDVYSFGILTWAVFAGREAE..................................................
Danio_rerio        : DEGGTLSYMPPEALQSSSYKPSKAFDVYSYGILLWSIITGKEPYSGVQSSLVRFRI.PLGDRPDLASV..DCSETEGLDELLKLMMQCWDQEPHR

                     1278                1298
Homo_sapiens       : RPSFQECLPKTDEVFQMVENNMNAAV
Pan_troglodytes    : RPSFQECLPKTDEAFQMVENNMNAAV
Mus_musculus       : RPSFQDCEPKTNEVYNLVKDKVDAAV
Rattus_norvegicus  : RPSFQDCESKTNNVYILVQDKVDAAV
Canis_familiaris   : RPSFQECQPITEEALNLVNKEMDAAV
Bos_taurus         : ........................
Danio_rerio        : RPSFLDC................
```

Figure S7. The Phosphorylation Site of RIP3 Is Conserved among Species, Related to Figure 7

(A) Wild type mouse RIP3 (WT) and the kinase-dead and phosphorylation site mutant (correlating to S227 of human RIP3) were transfected into NIH/3T3 cells. At 24 hrs posttransfection, the cells were treated as indicated for 24 hrs. Cell viability was determined by measuring ATP levels. The data are presented as the mean ± standard deviation of duplicate wells. Vector control: vec; kinase dead form RIP3: D143N, D161N; nonphosphorylation site mutant: T231A; phosphorylation site mutant RIP3 (S232A).

(B) Alignment of amino acid sequences of RIP3 orthologs in seven vertebrate species. Identical amino acid residues in the sequences are shaded in black. Amino acid residues conserved in 80% or more of the sequences are shaded in grey. The putative phosphorylation residue is denoted by asterisks (*).